

T.C.
AYDIN ADNAN MENDERES UNIVERSITY
GRADUATE SCHOOL OF NATURAL AND APPLIED SCIENCES
MASTER'S PROGRAMME IN CIVIL ENGINEERING
2021-YL-034

**AXIAL BEHAVIOR OF FRP CONFINED SQUARE
COLUMNS WITH POLYUREA**

SELIN TAYLAN
MASTER'S THESIS

SUPERVISOR

Assoc. Prof. Dr. Emre AKIN

This thesis was supported by Aydin Adnan Menderes University Scientific Research Projects Unit (Project number MF20012)

AYDIN-2021

ACKNOWLEDGEMENTS

Firstly, I acknowledge warmly my advisor, Associate Professor Doctor Emre Akin, for his patience, interest and guidance in this process. I would like to thank Instr. Dr. Burhan Aleessa Alam, who carried out the coupon tests in my study, for his positive contributions.

I appreciate my family and my friends for their trust and support. Also, I would like to thank Adnan Menderes University for the opportunity it provided during my research.



Selin TAYLAN

TABLE OF CONTENTS

APPROVAL AND ACCEPTANCE	ii
ACKNOWLEDGEMENTS	iii
TABLE OF CONTENTS	iv
LIST OF SYMBOLS AND ABBREVIATIONS	vi
LIST OF FIGURES	viii
LIST OF PICTURES	x
LIST OF TABLES	xi
ÖZET	xii
ABSTRACT	xiv
1. INTRODUCTION	1
1.1. Purpose and Subject of the Thesis	5
2. LITERATURE REVIEW	8
3. MATERIAL AND METHODS	11
3.1. Preparation and Application of Concrete	11
3.2. Test Specimens	13
3.3. Strengthening Specimens with GFRP and Polyurea	16
3.4. Test Setup	20
4. TEST RESULTS	23
4.1. Failure Modes	23
4.2. Axial Stress-Strain Response	26
4.3. Test Results	37
5. MODEL PREDICTIONS	45
5.1. Modeling for FRP Confined Circular Cross Sections	45

5.2. Modeling for FRP Confined Square Sections	46
6. DISCUSSION.....	52
6.1. Effect of Corner Radius.....	52
6.2. Effect of Number of Layers.....	53
6.3. Effect of Polyurea Coating	53
6.4. Comparison with The Existing Model	54
7. CONCLUSIONS	56
8. REFERENCES	59
9. CURRICULUM VITAE.....	64



LIST OF SYMBOLS AND ABBREVIATIONS

A_e	: Effectively confined area
A_e	: The total cross-sectional area
A_e/A_c	: Effective confinement area ratio
AFRP	: Aramid fiber reinforced polymers
A_g	: Gross area of the specimen
ASTM C39	: Standard test method for compressive strength of cylindrical concrete specimens
ASTM D3039	: Standard test method for tensile properties of polymer matrix composite materials
b-h	: Column width and height
BFRP	: Bazalt fiber reinforced polymer
CFRP	: Carbon fiber reinforced polymer
d	: Specimen diameter
D	: Diagonal distance of the section
EMPA	: Swiss Federal Materials Testing and Research Laboratories
ϵ_{cu}	: The ultimate strain for confined concrete
$\epsilon_{cu}/\epsilon_{co}$: Strain-enhancement ratio
ϵ_{co}	: The ultimate strain for unconfined concrete
ϵ_{fu}	: Rupture strain of fiber
E_{frp}	: Modulus of elasticity of fiber reinforced polymers
ϵ_{hrup}	: Hoop rupture strain
f_{cc}	: Compressive strength of confined concrete
f_{cc}/f_{co}	: Strength-enhancement ratio
f_{co}	: Compressive strength of unconfined concrete

f_u	: The confining pressure
FFR	: Flex fiber reinforced polymer
FRP	: Fiber reinforced polymer
GFRP	: Glass fiber reinforced polymer
IMO	: The Turkish of Chamber of Civil Engineers
k_{s1}	: The shape factor of strength-enhancement coefficient
k_{s2}	: The shape factor of strain-enhancement coefficient
k_1	: The strength-enhancement coefficient
k_2	: The strain-enhancement coefficient
LVDT	: Linear variable displacement transducers
NP	: None polyurea
P	: Polyurea
R	: Radius
S	: Unconfined concrete specimens
SRef	: Confined reference specimen
t_f	: Nominal thickness of fiber reinforced polymer
σ_u	: Tensile strength, ultimate tensile strength

LIST OF FIGURES

Figure 3.1. The details of test specimens (3D forms).....	14
Figure 3.2. The details of the corner radius of specimens (2D forms).....	15
Figure 3.3. Stress-strain diagram of coupon test results.....	20
Figure 4.1. Theoretical stress-strain curves for confined and unconfined concrete.....	27
Figure 4.2. Stress-strain curve for unconfined concrete.....	28
Figure 4.3. Stress-strain curve for the specimen SRef-2G-NP.....	28
Figure 4.4. Stress-strain curves for group of S15-1G-NP.....	29
Figure 4.5. Stress-strain curves for group of S15-1G-P.....	29
Figure 4.6. Stress-strain curves for group of S15-2G-NP.....	30
Figure 4.7. Stress-strain curves for group of S15-2G-P.....	30
Figure 4.8. Stress-strain curves for group of S30-1G-NP.....	31
Figure 4.9. Stress-strain curves for group of S30-1G-P.....	31
Figure 4.10. Stress-strain curves for group of S30-2G-NP.....	32
Figure 4.11. Stress-strain curves for group of S30-2G-P.....	32
Figure 4.12. Stress-strain curves for group of EC-1G-NP.....	33
Figure 4.13. Stress-strain curves for group of EC-2G-NP.....	33
Figure 4.14. Axial stress-strain diagram of comparison between S15-1G-NP and S30-1G-NP.....	34
Figure 4.15. Axial stress-strain diagram of comparison between S15-1G-P and S30-1G-P...	34
Figure 4.16. Axial stress-strain diagram of comparison between S15-2G-NP and S30-2G-NP.....	35
Figure 4.17. Axial stress-strain diagram of comparison between S15-2G-P and S30-2G-P...	35
Figure 4.18. Axial stress-strain diagram of S15 group.....	36
Figure 4.19. Axial stress-strain diagram of S30 group.....	36

Figure 4.20. Hoop rupture strain diagram for SRef-2G-NP	38
Figure 4.21. Hoop rupture strain diagram for S15-1G-NP group	39
Figure 4.22. Hoop rupture strain diagram for S15-1G-P group	39
Figure 4.23. Hoop rupture strain diagram for S15-2G-NP group	40
Figure 4.24. Hoop rupture strain diagram for S15-2G-P group	40
Figure 4.25. Hoop rupture strain diagram for S30-1G-NP group	41
Figure 4.26. Hoop rupture strain diagram for S30-1G-P group	41
Figure 4.27. Hoop rupture strain diagram for S30-2G-NP group	42
Figure 4.28. Hoop rupture strain diagram for S30-2G-P group	42
Figure 4.29. Hoop rupture strain diagram for EC-1G-NP group.....	43
Figure 4.30. Hoop rupture strain diagram for EC-2G-NP group.....	43
Figure 5.1. Illustration of the proposed model for FRP-confined square sections.....	46
Figure 5.2. Comparison of experimental results and model predictions for strength-enhancement (considering rupture strain from the tests of specimens with square section)	49
Figure 5.3. Comparison of experimental and model predictions for strength-enhancement (considering rupture strain from the tests of specimens with equivalent circular section)	49
Figure 5.4. Comparison of experimental results and model predictions for strain-enhancement (considering rupture strain from the tests of specimens with square section)	50
Figure 5.5. Comparison of experimental and model predictions for strain-enhancement (considering rupture strain from the tests of specimens with equivalent circular section).....	50

LIST OF PICTURES

Picture 1.1. The column confined by a new reinforced concrete layer (Altin, 2008)	2
Picture 1.2. Column reinforced with steel confinement (Yilmaz, 2006).....	3
Picture 1.3. Different types of FRP samples; GFRP, FFRP, CFRP	4
Picture 3.2. a)Placing the concrete in the mold, b)Demoulded specimens	12
Picture 3.3 a) and b) The polyester brackets as attached at the corners of the molds, c) The polyester brackets.....	15
Picture 3.4. a) Preparing the caps of a specimen, b) Specimens with caps	16
Picture 3.5. a) The components of primer, b) Specimens after the application of primer, c)The components of epoxy, d) The confined and unconfined specimens	17
Picture 3.6. a) The primer used before polyurea application, b) The components of polyurea, c) Primer application, d) Polyurea application.....	17
Picture 3.7. a) The polyurea applied specimen, b) The polyurea coated specimens; S15-1G-P and S15-2G-P, c) The polyurea coated specimens; S30-1G-P and S30-2G-P.....	19
Picture 3.8. Strain gauge application stages	21
Picture 4.1. The failure mode of specimen, SRef-2G-NP	23
Picture 4.2. Failure modes of S15-1G-NP and S15-1G-P groups	24
Picture 4.3. Failure modes of S15-2G-NP and S15-2G-P groups	24
Picture 4.4. Failure modes of S30-1G-NP and S30-1G-P groups	25
Picture 4.5. Failure modes of S30-2G-NP and S30-2G-P groups	26
Picture 4.6. a) Failure modes of EC-1G-NP group, b) Failure modes of EC-1G-P group.....	26

LIST OF TABLES

Table 3.1. Concrete design mixing ratios	11
Table 3.2. Test matrix	14
Table 3.3. The mechanical properties of the high-strength mortar.....	15
Table 3.4. The mechanical properties of the epoxy	17
Table 3.5. The mechanical properties of the cold polyurea.....	18
Table 3.6. Coupon test results.....	20
Table 4.1. The test results	44
Table 5.1. The strength- and strain enhancement ratios predicted by Lam and Teng (2003b)	51

ÖZET

POLYUREA İLE TAKVIYE EDİLMİŞ FRP SARGILI KARE KOLONLARIN EKSENEL DAVRANIŞI

Taylan S., Aydın Adnan Menderes Üniversitesi, Fen Bilimleri Enstitüsü, İnşaat Mühendisliği Programı, Yüksek Lisans Tezi, Aydın, 2021.

Amaç: Çalışmanın amacı düşük dayanımlı betonda cam FRP (GFRP) ile sağlanan sargılamının etkinliğinin artırılmasında polyurea etkisini irdelemektir.

Materyal ve Yöntem: Bu çalışma için 106 mm x 106 mm kesit boyutlarında ve 300 mm yüksekliğinde 23 adet kare kolon numune üretilmiştir. Kare kolonların keskin köşeleri, 15 mm veya 30 mm köşe yarıçapı ile yuvarlatılmıştır. Böylelikle keskin köşelerde gerilim yoğunlaşması önlenmiştir. Çıplak beton dayanımını hesaplayabilmek için iki adet kare numune sargılanmamıştır. Diğer örnekler tek ve çift katmanlı GFRP ile sargılanmıştır. Eksenel basınç altında sargılama üzerinde daha uniform bir enine birim şekil değiştirme dağılımı sağlamak amacıyla on adet numune sargılanmadan önce polyurea ile kaplanmıştır. Tüm numuneler, monotonik eksenel basınç yüklemesi altında test edilmiştir. Test sonuçları, mevcut bir tasarım odaklı modelin maksimum gerilim ve birim deformasyon kapasitesi hesaplarıyla karşılaştırılmıştır. Ayrıca kare numunelerin diyagonal uzunluğuna (yani 150 mm) eşit bir çapa sahip altı adet silindirik beton numunesi üretilmiştir. Silindirik numuneler, bir veya iki katmanlı GFRP ile sargılanmıştır. Bu “eşdeğer silindirik” numunelerin monotonik eksenel basınç test sonuçları model tahminlerinde kullanılmıştır.

Bulgular: Eksenel monotonik gerilme-birim şekil değiştirme eğrileri test sonuçlarından elde edilmiştir. Maksimum basınç dayanımı, maksimum eksenel ve yanal birim deformasyon değerleri belirlenmiştir. Ek olarak, gerilme ve birim şekil değiştirme artış oranları hesaplanmıştır. Numunelerin maksimum eksenel dayanımı ve birim deformasyon kapasitesi de tasarım odaklı model tarafından tahmin edilmiş ve deneysel bulgularla karşılaştırılmıştır.

Sonuç: Basınç dayanımındaki en iyi gelişme, 30 mm yuvarlatılmış köşeli iki katmanlı GFRP ile sargılanmış (yani S30-2G-NP) numunelerde gözlenmiştir. Öte yandan, polyureanın katkısı en iyi, 15 mm yuvarlatılmış köşeli tek katmanlı sargılı (yani S15-1G) örneklerde görülmüştür. Bu örneklerin enine kopma birim deformasyon değerlerinde de bir iyileşme gözlenmiştir. Yine de, genellikle silindirik numuneler için geçerli olan yanıl gerilimin homojen dağılımı, polyurea kaplamaya rağmen kare kolon numunelerde elde edilememiştir.

Anahtar Kelimeler: GFRP, Güçlendirme, Kare Kolonlar, Polyurea



ABSTRACT

AXIAL BEHAVIOR OF FRP CONFINED SQUARE COLUMNS WITH POLYUREA

**Taylan S., Adnan Menderes University, Graduate School of Natural and Applied Science,
Civil Engineering Program, Master's Thesis, Aydin, 2021.**

Objective: The aim of this study was to investigate the effect of polyurea in increasing the efficiency of GFRP confinement for the low-strength concrete.

Materials and Methods: For this study, 23 square column specimens with 106 mm x 106 mm cross-sectional sizes and a height of 300 mm were produced. The sharp corners of the square columns were rounded by either 15 mm or 30 mm corner radius. Thus, stress concentrations on sharp corners are prevented. Two of the square specimens were not confined to calculate the bare concrete strength. Other specimens were confined with single and double GFRP fabrics. Ten specimens were coated with polyurea before being confined with the aim of providing more uniform hoop strain distribution on the confining jacket under axial compression. All specimens were tested under monotonic axial compressive loading. The test results were compared with the ultimate strength and strain capacity predictions of an existing design-oriented model. Six cylindrical concrete specimens with a diameter that equals to the diagonal length of square specimens (i.e. 150 mm) were produced. The cylindrical specimens were confined by either one- or two-layers of GFRP. The monotonic axial test results of these “equivalent cylindrical” specimens were utilized in the model predictions.

Results: The axial monotonic stress-strain curves were obtained from the test results. The ultimate compressive strength, maximum axial and lateral strains were determined. In addition, stress- and strain- enhancement ratios were calculated. The ultimate axial strength and strain capacity of the specimens were also predicted by the design-oriented model and compared with the experimental findings.

Conclusion: The highest improvement in the compressive strength was observed in the specimens having two-layers of GFRP confinement with 30 mm rounded corners (i.e. S30-2G-NP). On the other hand, the contribution of polyurea was best observed in the specimens having one-layer of confinement with 15 mm rounded corners (i.e. S15-1G). There was also an improvement in the hoop rupture strains of these specimens. Still, the homogeneous distribution of the lateral strain which is generally the case for the cylindrical specimens could not be obtained despite the polyurea coating.

Key Words: GFRP, polyurea, strengthening, square columns



1. INTRODUCTION

Located in one of the active earthquake zones, Turkey is exposed to frequent and major earthquakes. Since the past earthquakes have caused serious property and loss of lives. As a result of these earthquakes, a significant deficient building stock has been formed in our country. It is not possible to expect that these earthquakes will not occur in the future. Deficient structures in the building stock may cause great danger for future earthquakes. For this reason, it is very important to detect deficient structures and to take the necessary precautions.

The causes of damage in buildings under seismic effects. The reasons of damages in the buildings in the case of an earthquake can be listed as:

- i. non-compliance to the building code provisions,
- ii. design/construction errors (especially errors in reinforcement design)
- iii. lack of lateral rigidity,
- iv. use of low-quality concrete,
- v. labor errors,
- vi. short column effect,
- vii. soft storey factor,
- viii. designs that are not suitable for the ground (i.e. soil),
- ix. structural systems with the weak column-strong beam.

Structures with such deficiencies need to be strengthened. A strategy should be determined for the strengthening according to Tankut (2005). Firstly, the reasons for the weakness of the building should be determined, then the targeted safety level should be decided. In this way, the method for the strengthening of the structure or structural element should be decided. (Tankut, 2005)

Structural strengthening methods can be evaluated in two main categories. The first is to improve structural performance and save it from earthquake effects. This refers to the system rehabilitation. On the other hand, if the insufficient structural elements are to be improved individually, that calls member strengthening.

The main purpose of system rehabilitation is to increase the strength, rigidity and deformation capacity (i.e. ductility) of the system and to ensure continuity in the distribution

of internal forces. In this direction, adding new structural elements such as shear walls, the new reinforced concrete frame can ensure that existing elements carry a lower load. Or the earthquake loads can be reduced by reducing the mass of the building.

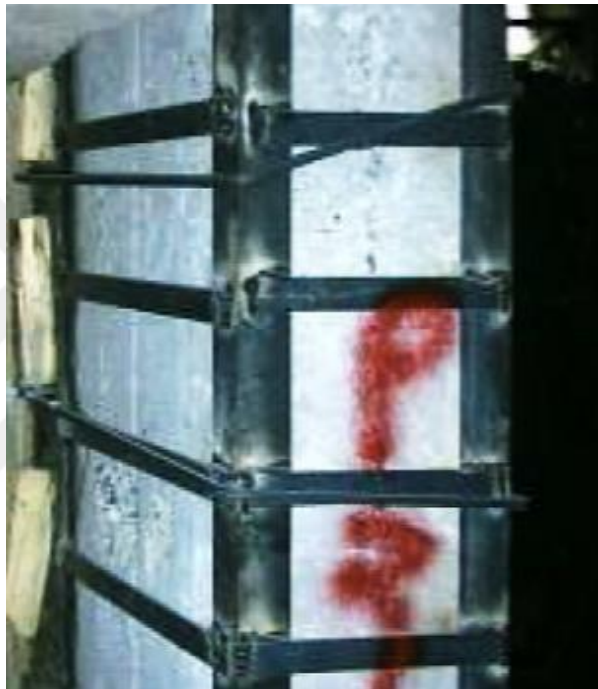
In the member strengthening technique, the columns, beams and joints carrying earthquake loads are improved in terms of strength and ductility. Since the columns must be regarded as the most critical members for the seismic strengthening. In the strengthening of the columns, different strategies and methods can be chosen with different purposes. The strengthening can be applied for the axial, shear and/or flexural response. The confinement of the columns can be enhance to improve the ductility, axial and shear strength of the columns which by adding a new reinforced concrete layer, steel braces or wrapping by the fiber-reinforced polymers. The advantages and disadvantages of these methods are detailed in the following paragraphs.

The reinforced concrete jacketing (RC) method is the enlargement of the column cross section by creating a new well-equipped reinforced concrete layer around the existing reinforced concrete column. This method is effective in increasing the axial load carrying capacity of the column. RC jacketing is effective in increasing shear strength and insufficient lapped length of longitudinal reinforcement. However, the difficulties during the implementation stage are the downside of this application. Besides, since this method increases the weight of the structure significantly, it makes it necessary to control the system behavior. Picture 1.1 shows an example of a column with RC jacketing.



Picture 1.1. The column confined by a new reinforced concrete layer (Altin, 2008)

According to the Turkish Earthquake Code (2018), the confinement formed by placing four brackets at the corners of the reinforced concrete columns which are connected by the welded lateral steel plates at a defined spacing is termed as strengthening by steel sections. No gap should be left between the reinforced concrete surface and steel angle brackets. With this strengthening method, the ductility and load carrying capacity of the column increases. However, if the angle brackets are not tightened well, the desired design capacity cannot be reached. The moment transfer cannot be made with steel confinement. It is not a highly preferred method due to its insensitivity to fire and its high cost (Picture 1.2).



Picture 1.2. Column reinforced with steel confinement (Yilmaz, 2006)

Another material to be used for the confinement of concrete is fiber-reinforced polymer (FRP). The composite materials formed by impregnating the fiber produced with a special process using resin (epoxy, polyester) are called fiber-reinforced materials. Aim of confinement is to enhance the axial properties of the concrete by means of confinement ductility and compressive strength is supported be increased (Lam and Teng, 2003b; Ozbakkaloglu and Akin, 2012). Major FRP types are carbon fiber (CFRP), glass fiber (GFRP), aramid fiber (AFRP) and basalt fiber (BFRP). In Picture 1.3 shows that different types of FRP samples. Despite their high cost, these FRP types are widely used in many areas. This is due to its effective properties such as lightness, high-strength and corrosion resistance (Cao et al., 2020; Stylianidis and Petrou, 2019). First researches and applications

in this field were carried out in Switzerland, Germany and Japan. By the year 1980, many experimental research and repair or strengthening processes have been carried out in the structures in the field projects. Likewise, by the year 1990, the positive results that emerged with the influence and contributions of the United States of America, Canada and Saudi Arabia have excited structural engineers (Buyukozturk, 2000).



Picture 1.3. Different types of FRP samples; GFRP, FFRP, CFRP

It is necessary to understand the mechanical properties and working principles of FRP composite types for the correct selection of application areas. The main difference between these materials is due to their stiffness and tensile strength. The glass fibers which were used in this study are obtained by mixing silica sand, limestone, folic acid and other small components. The mixture is heated at about 1260 °C until it melts. The glass strips are cooled, collected and wound. The fibers are pulled to transfer forces. The fibers are then woven for use in composites. The glass fibers have high electrical insulation, low moisture resistance and high mechanical properties. For these reasons, it is considered the dominant reinforcement for polymer matrix composites. On the other hand, even though GFRP is resistant to impacts, it is heavier than carbon and aramid.

The carbon fibers have a high modulus of elasticity of about 200-800 GPa. The ultimate elongation is 0.3-2.5% where the lower elongation corresponds to the higher stiffness and vice versa. The carbon fibers are resistant to moisture and chemical solutions. They are also resistant to fatigue. On the other hand, they do not show abrasion, creep and loosening.

Aramid is a short form of aromatic polyamide. Fiber modules are 70-200 GPa with a final elongation of 1.5-5 % depending on the grade. Because aramid has high fracture energy, it is mostly used in helmet and bullet-proof clothing manufacturing. Due to their sensitivity

to high temperatures, humidity and ultraviolet radiation, it is not widely used in civil engineering applications. Also, aramid fibers have problems with relaxation and corrosion.

The retrofitting of structural members with FRP composites was first considered as a research subject in the early 1980s in Japan, which is located in an intense earthquake zone. It was revealed that the FRP materials were used for seismic retrofitting of columns in 1985, chimneys in 1986, and bridge columns in 1989 (Kobatake, 1998). The first repair process with composite was carried out by Ballinger (1997) in 1997 and Fukuyama et al. (1997) in 1997 by covering the cracks in the bridge piers of a railway with CFRP plates. With the contribution of this application, the disadvantages of traditional repair methods have been understood.

In Europe, the research and use of FRP composites for the repair and reinforcement began in the early 1990s. While the Swiss Federal Materials Testing and Research Laboratories (EMPA) focused on CFRP composites, the Technical University of Braunschweig in Germany focused on GFRP composites. The first field application in Europe was made in 1991 on the Ibach Bridge in Lucerne, Switzerland (Buyukozturk, 2000).

1.1. Purpose and Subject of the Thesis

In the previous section, the strengthening techniques, which were divided into two main categories, were examined in detail. As can be seen from the history of the practical use and research of FRP materials, these materials have been in our lives for years. The high tensile strength to weight ratio, corrosion resistance, general durability and ease of application of FRP materials accelerated the use of these materials in construction industry.

In the recent years, the confinement of concrete with FRP composites to enhance its axial behavior has become popular in structural engineering. The initial researchers have focused on the cylindrical column specimens (Lam and Teng, 2003a; Wu et al., 2006) These studies have revealed the efficiency of this material to enhance the axial strength and ductility of concrete. Even in the cylindrical specimens, the efficiency of FRP is reduced by early rupture of these materials before reaching their actual rupture strain capacity that is given by the manufacturer or obtained from the tensile coupon tests. A number of reasons have been asserted, including the local stress concentrations caused by the irregular

damaging of the concrete under axial loads (Lam and Teng, 2003a). In the previous study by Akin et al. (2020), the polyurea material with high bonding, tear and elongation capacities was used as a padding material between FRP and circular column section to increase FRP confinement efficiency. This study showed that the polyurea coating prevented local stress concentrations on the FRP due to damaging concrete, especially under cyclic axial loading. And this enabled FRP to be used more efficiently with improved rupture strain capacity. Besides, it was reported that a more uniform hoop strain distribution, which is more compatible with the theoretical assumptions of design-oriented models, may be provided by utilizing the polyurea layer.

On the other hand, majority of the columns in the building stock has a square or rectangular cross-sectional shape rather than circular. Therefore, a significant number of research projects investigated the axial behavior FRP confined concrete specimens having these sections (Bakis et al., 2002; CEB-fib, 2001; Ozcan et al., 2010; Ozbakkaloglu and Oehlers, 2008; Priestley et al., 1996; Sharma et al., 2013; Wang and Wu, 2008; Zhong et al., 2008). The major problem for the confinement of concrete having square or rectangular section is the additional stress concentration that takes place at the sharp edges. This problem has been solved by rounding the corners of the section. Yet, the stress concentrations cannot be removed completely leading to a confinement efficiency that is not as high as the one applied in an equivalent circular section (Lam and Teng, 2003b).

In this thesis study, the polyurea coating was applied on the concrete specimens having a square section before the GFRP wrapping. It was aimed to reduce the previously mentioned stress concentrations and increase the performance of GFRP as a confining material for the concrete with square section. Therefore, an experimental study was conducted where monotonic axial loading was applied on the concrete specimens. The sharp edges of the test specimens were rounded by 15 mm or 30 mm corner radius. Besides, one- or two-layers of GFRP confinement was considered. The test results are evaluated in terms of observed failure type, overall axial response, ultimate axial strength and strain capacity. Eventually, the test results were compared with predictions of a design-oriented model (Lam and Teng, 2003b) for the square sections confined by FRP.

The study is summarized as follows in the sections below.

- Chapter 2 provides reviews of studies dealing with the reinforcement of square columns with FRP composites. There is also a study examining the effect of polyurea by Akin et al. (2000), which forms the basis of this study.
- Chapter 3 describes the material properties used in the study, the matrix of test program, the fabrication/strengthening process, and the test setup.
- Chapter 4 includes test results in light of observed behavior, taking into account the notes and pictures taken during the experiments. Also, the failure modes, stress-strain curves and ultimate conditions of the test specimens are presented.
- Chapter 5 explains the numerical design-oriented model suggested by Lam and Teng (2003b) for the specimens with square sections. The resulting axial strength- and strain-enhancement ratios predicted by the model for the test specimens are given in tables and compared with the test results.
- Chapter 6 discusses the experimental test results and comparison of the model predictions with test results.
- Chapter 7 summarizes the conclusions which were inferred as a result of this study.

2. LITERATURE REVIEW

A significant number of researches have been conducted on the FRP confinement of concrete in the last decades. The researchers considered many parameters that may influence the axial behavior of concrete confined by FRP. Some of these variables are the size, aspect ratio and geometry of the specimens, unconfined concrete strength, number or type of FRP layers, orientation of fibers, corner radius in the square/rectangular sections, overlap length.

Mirmiran et al. (1998) examined the effects of specimen shape, specimen length and bond of FRP confined-concrete. They observed that square specimens were less effective in confinement than their circular counterparts. They concluded that this effectiveness depends on the corner radius. Also, the adhesive bond did not increase the load-carrying capacity of the FRP-confined specimen. However, the mechanical bond confinement contributed positively to the specimen by effectively distributing the pressure.

Paula and Silva (2002) investigated the effect of the corner radius of reinforced concrete square columns on the FRP wrapping. Specimens with cylindrical, sharp corners, 20 mm and 38 mm rounded corners are wrapped with CFRP. According to the uniaxial compression test results, it was observed that the increase in the corner radius and the increase of ultimate strength were directly proportional. Moreover, they concluded that even the sharp-edged square specimen confined with CFRP increased axial deformation capacity eight times compared to unconfined concrete (Paula and Silva, 2002).

Lam and Teng (2003b) investigated the response of FRP confined square and rectangular specimens in comparison to the cylindrical specimens. A database was created with the results of many previous tests and tests made by the authors of this study. The new test results, a design-oriented model was suggested for the FRP confined concrete with square/rectangular sections as a result of these results. Besides, the suggested model was assessed by comparing the predicted results with the new test results. The obtained results showed that the suggested model predictions were satisfactory (Lam and Teng, 2003b).

Al-Salloum (2007) studied the effects of the corner radius of square columns on the FRP confinement. Twenty specimens were tested with a uniaxial compression test. The study consisted of two stages, numerical and experimental. According to the test results, flattening the edges of the square section plays an important role in delaying the rupture of the FRP composite on these edges. It is also concluded that the effectiveness of the FRP is directly

related to the radius of the cross-section edges. An analytical model was developed to estimate the strength of FRP confined concrete with the circular, as well as rounded square sections. It has been observed that the predicted results are in perfect agreement with the measured results (Al-Salloum, 2007).

Tao et al. (2008) performed axial compression tests on CFRP-wrapped rectangular specimens. According to the test results, the authors concluded that CFRP wrapping has more effective in the low-strength concrete. They also stated that the confinement efficiency has directly proportional to the corner radius and that the confinement of the concrete increases as the number of CFRP layers increases (Tao et al., 2008).

Ozbakkaloglu and Oehler (2008) studied the behavior of square and rectangular concrete-filled FRP tubes under concentric compression. FRP tubes were designed as column confinement reinforcement. The research examines the effect of tube thickness and corner radius, cross-sectional aspect ratio and concrete strength on the FRP confinement. The results show an improvement in the ductility for both square and rectangular columns. The results also show that the confinement efficiency of FRP tubes is higher in the square columns and the efficiency increases along with the corner radius in both types of sections (Ozbakkaloglu and Oehler, 2008).

Sharma et al. (2013) investigated the effect of corner radius and number of layers for the small-scale square column specimens on the confinement efficiency of GFRP. 15 square reinforced concrete columns with cross-sectional dimensions of 125 mm × 125 mm and length of 1200 mm were tested under axial compression. The corners of the specimens were rounded by 5 mm and 25 mm radius to prevent premature rupture. The column specimens with 25 mm corner radius gave better results than other specimens in terms of ultimate load-carrying capacity (Sharma et al., 2013).

Akin et al. (2020) investigated the effect of polyurea to enhance the effectiveness of FRP confinement. The polyurea layer between the concrete and FRP jacket was supposed to reduce the stress concentrations caused by the irregular lateral deformations of concrete under axial compression. Thus, the early rupture of the FRP jacket was aimed to be increased by providing a more uniform hoop strain distribution. In the study, 28 low-strength specimens were used. The specimens were tested under monotonic or cyclic axial compression. It was observed that polyurea had a positive contribution to the ductility under

axial loading. In addition, this contribution was more considerable in the cyclic axial compression test results (Akin et al., 2020).



3. MATERIAL AND METHODS

In this section, the detailed information is given about all the materials that were used in this study. The specifications and preparation stages of the specimens are explained. The test setup and methodology are also described at the end of the section.

3.1. Preparation and Application of Concrete

The concrete to be used in the square section specimens was planned to have a low compressive strength (approximately 10~15 MPa) to represent the concrete grade in target existing substandard buildings. For this reason, the low strength concrete mixture has been prepared with the design mixing ratios given in Table 3.1.

Table 3.1. Concrete design mixing ratios

Materials	Fine Aggregate	Coarse Aggregate (maximum diameter =15 mm)	Cement	Water	Total
Weight Ratio (%)	19	58	12	11	100

The molds for the square concrete specimens were prepared by using 20 mm thick plywood plates. The pieces of plywood plates were joined by the screws. Picture 3.1 shows the prepared molds.



Picture 3.1. The prepared plywood molds

Before casting the concrete, the inner surfaces of the molds were oiled. This prevents concrete from sticking to the mold, allowing it to be easily removed from the mold. The concrete was placed into the molds in three fractions. Each concrete fraction was compacted by using tamping rods to avoid honeycombs in the specimens. The top of the specimens was smoothed to obtain a plain surface (Picture 3.2.a). The demoulded specimens are shown in Picture 3.2.b.



Picture 3.2. a) Placing the concrete in the mold, b) Demoulded specimens

After three days, the specimens were demoulded. Since the specimens were planned to be low-strength concrete, only the water was sprayed on the specimens for seven days for curing. After approximately 28 days of concrete casting, the axial compression tests were carried out at the Adnan Menderes University Civil Engineering Laboratory.

3.2. Test Specimens

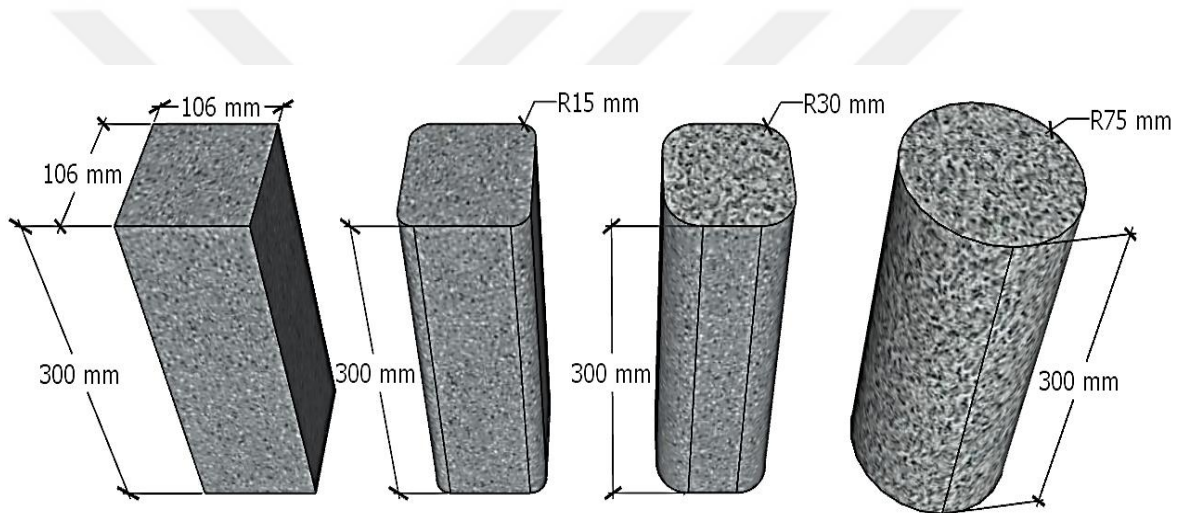
For this study, 23 specimens with square sections having 106 mm side length and 6 cylindrical specimens with a diameter of 150 mm were designed for the tests. All specimens had a height of 300 mm. The test results of cylindrical specimens were used in the numerical model predictions according to Lam and Teng (2003b). The diameter of these specimens with “equivalent circular” sections were arranged to be equal to the diagonal length of the square specimens (Lam and Teng, 2003b). The corners of twenty square specimens were rounded by either 15 or 30 mm to prevent stress concentrations and premature rupture of confining jacket (Lam and Teng, 2003b; Santos et al., 2013; Yang et al., 2001). Twelve specimens had a corner radius of 15 mm. Whereas eight of them had 30 mm corner radius. Two of the specimens with square section were tested to serve as unconfined reference specimen (i.e. SRef). One square specimen with no rounded corners was also tested as a reference specimen to highlight the effect corner rounding (i.e. SRef-2G-NP). This specimen confined by two layers of GFRP where no polyurea application was provided. There were three main test parameters for the square specimens including the corner radius of square specimens (15 mm or 30 mm), whether to use polyurea or not (P or NP, respectively) and the number of GFRP layers (one or two layers). On the other hand, there is only one test variable, the number of FRP layers, for the cylindrical specimens.

In the labeling of the specimens, the first letters, S or EC designate the cross-sectional shape of specimens (square or equivalent circular). The numbers after the labels of square specimens represent the corner radius (15 mm or 30 mm). Then, the number of GFRP layers used for the confinement is mentioned as 1G and 2G for the one- and two-layers, respectively. And the final letters present whether the polyurea was used or not as P or NP, respectively. For example, S15-1G-NP is for a specimen with square section having 15 mm rounded corners and wrapped by one layer of GFRP without any polyurea application. All test parameters and classification of the specimens are shown in Table 3.2. The test specimens in different groups are illustrated in Figure 3.1.

Table 3.2. Test matrix

TEST GROUP	SPECIMENS	CORNER RADIUS (mm)	NUMBER OF FRP LAYERS	SPECIMEN NUMBER
SRef	SRef	-	-	2
	SRef-2G-NP	-	2	1
S	S15-1G-NP	15	1	3
	S15-1G-P	15	1	3
	S15-2G-NP	15	2	3
	S15-2G-P	15	2	3
	S30-1G-NP	30	1	2
	S30-1G-P	30	1	2
	S30-2G-NP	30	2	2
	S30-2G-P	30	2	2
EC	EC-1G-NP	-	1	3
	EC-2G-NP	-	2	3

*SRef: reference specimen with square section, S: strengthened specimen with square section, EC: equivalent specimen with a circular cross-section, P: with polyurea, NP: without polyurea, G: glass FRP

**Figure 3.1.** The details of test specimens (3D forms)

The sharp corners of the specimens have the potential to cause premature rupture of the FRP layers due to stress concentrations. Therefore, the corners were rounded as also mentioned previously. The details of the specimens having rounded corners are shown in Figure 3.2. The brackets were prepared for rounding the corners by casting polyester resin into the molds that were specially produced by 3D printing technology. The brackets made of polyester were attached at the corners of the wooden molds to provide a rounded edge. Picture 3.3 shows the details of this process.

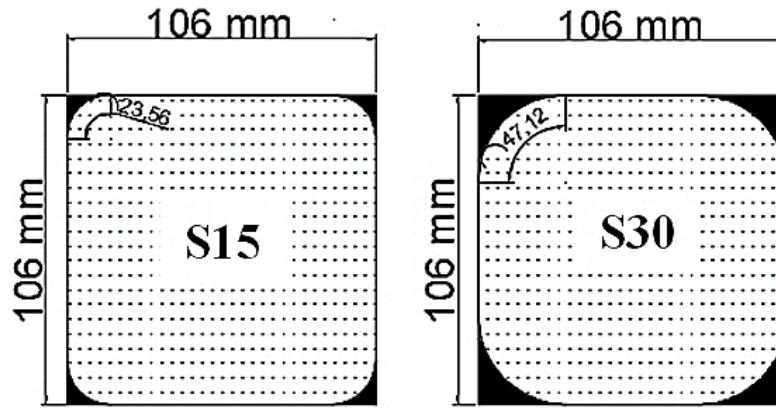
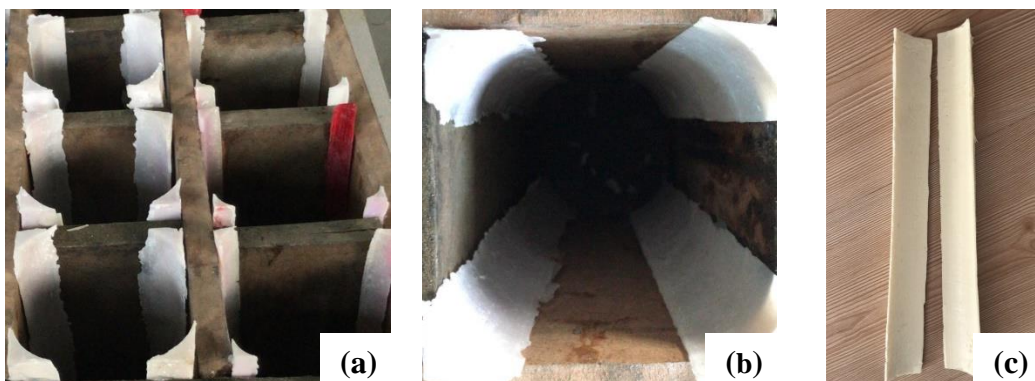


Figure 3.2. The details of the corner radius of specimens (2D forms)

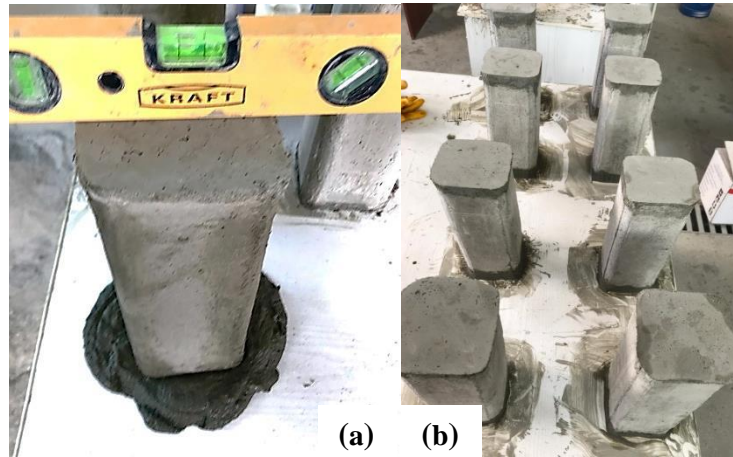
To provide a uniform axial stress distribution on the specimens is important during the compressive tests. For this reason, high strength mortar caps were applied to level the lower and upper surfaces of the specimens. Firstly, a clean (i.e. smooth) ground was determined. The specimen was brought to the same elevation as the surface with the help of a water balance after it was placed on the fresh mortar on this surface. Picture 3.4 shows how the caps of the specimens were prepared. Some important mechanical properties of the high-strength mortar is summarized in Table 3.3 as supplied by the manufacturer.

Table 3.3 The mechanical properties of the high-strength mortar

Compressive strength (MPa)	Modulus of elasticity (GPa)	Bonding strength to concrete (MPa)
>60 (28 days)	>20 (28 days)	>2 (28 days)



Picture 3.3 (a) and (b) The polyester brackets as attached at the corners of the molds, (c) the polyester brackets



Picture 3.4. (a) Preparing the caps of a specimen, (b) specimens with caps

3.3. Strengthening Specimens with GFRP and Polyurea

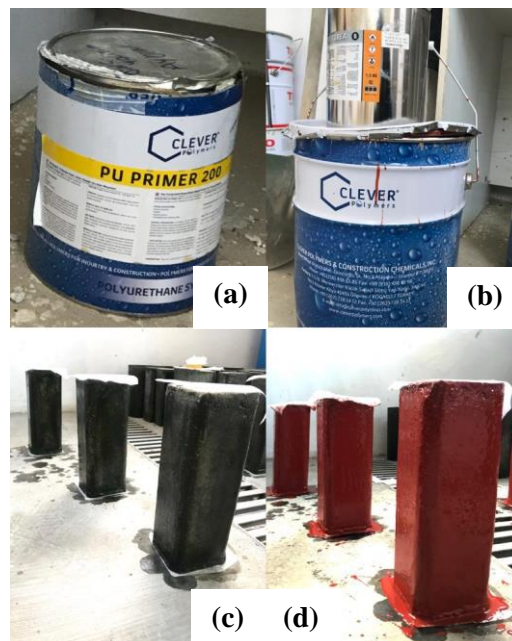
For the specimens without polyurea, the applied strengthening started with the application of a two-component liquid primer to provide a dust-free surface (Picture 3.5.a, b). One day after the application of primer, the GFRP fabrics were cut in the measured dimensions by considering an overlapping length of 150 mm for the confining jacket. The height of the GFRP fabrics were kept approximately 10 mm lower than the specimen height. It was aimed to provide an unconfined gap at both ends of the specimens after the confinement. This unconfined region and the high-strength mortar beyond was supposed to prevent any accidental axial stress transfer to the jacket and let the confinement strained only in the lateral direction. The two-component epoxy resin (Picture 3.5.c) was used for the FRP wrapping. The epoxy resin was applied both on the lateral surfaces of the specimens and the prepared GFRP fabrics by using a roller. Then, the epoxy impregnated GFRP fabrics were wrapped around the specimens (i.e. wet-lay-up technique). During wrapping, care was taken to ensure that the FRP fibers are in the lateral direction and that there is no gap between the specimen surface and GFRP jacket. The wrapped GFRP fabric ended after an overlapping zone along a length of 150 mm. In the double layer wrapping application, the 150 mm overlap was planned to end at the same place as the first layer. A specimen after the confinement is shown in Picture 3.5.d. Some important mechanical properties of the epoxy used for the GFRP confinement is given in Table 3.4 as supplied by the manufacturer.

Table 3.4 The mechanical properties of the epoxy

Compressive strength	≥ 80 MPa
Tensile strength	≥ 30 MPa
Adhesion to concrete	≥ 4 MPa
Mixing ratios by weight	Unit A: 2 and Unit B: 1



Picture 3.5. (a) The components of primer, (b) specimens after the application of primer, (c) the components of epoxy, (d) the confined and unconfined specimens

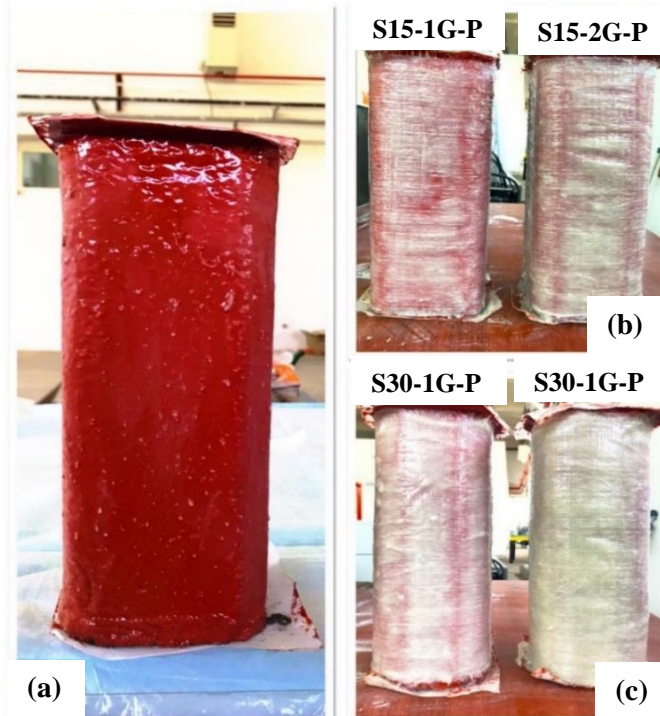


Picture 3.6. (a) The primer used before polyurea application, (b) the components of polyurea, (c) primer application, (d) polyurea application

The FRP jacketing is well-known to provide a significant improvement in the axial behavior of the concrete. However, it is also known that the FRP material ruptures prematurely before reaching its actual strain capacity due to various reasons (Lam and Teng, 2003a). One such reason of this phenomenon is explained as the stress concentrations on the FRP jacket caused by the deforming concrete under the confinement. Akin et al. (2020) used the polyurea as a padding material between the FRP and concrete by utilizing its superior adherence and tearing capacity (i.e. elongation at break). The main aim was stated to reduce the stress concentrations on the FRP jacket due to damaging concrete which was reported to be achieved in the cyclically loaded cylindrical specimens. Addition to the those caused by the deforming concrete, the stress concentrations are also known to take place at the sharp edges of FRP confined specimens with square/rectangular sections. To reduce all these effects and provide a more uniform lateral strain distribution on the confining jacket, the cold polyurea was applied on the surfaces of ten square specimens in different test groups. The single component primer for the polyurea (Picture 3.6.a) was applied initially on the concrete surface by using a roller in these specimens (i.e. before the GFRP wrapping). After waiting for 3-4 hours as suggested by the manufacturer, the liquid cold polyurea was applied on the primer coated surface again by using a roller. The polyurea used in this study has two-components which were mixed in room temperature (Picture 3.6.b). Also Picture 3.6.c shows specimen with primer. After 3-4 hours, a new layer of polyurea was formed on the previous one. At the end, the thickness of the polyurea was approximately 2-3 mm (Picture 3.6.d). Some important mechanical properties of the cold polyurea used prior to the GFRP confinement is provided in Table 3.5 as supplied by the manufacturer.

Table 3.5 The mechanical properties of the cold polyurea

Elongation at break	$\geq 600\%$
Tensile strength	$\geq 9 \text{ MPa}$
Adhesion to concrete	$\geq 2 \text{ MPa}$



Picture 3.7. (a) The polyurea applied specimen, (b) the polyurea coated specimens, S15-1G-P and S15-2G-P (c) the polyurea coated specimens, S30-1G-P and S30-2G-P.

One day after the polyurea application, these specimens were confined with GFRP fabrics by using the same wet-lay-up technique as explained before. The only difference was that no two-component primer was used for the epoxy in this case, since the polyurea already provides a dust-free surface. In Picture 3.7.b and c, the FRP confined specimens after the polyurea application are shown.

The tensile properties of the GFRP jacket was obtained by the coupon tests. For testing, four flat coupons with a single layer of GFRP were prepared. These coupon's width and height were 15 mm and 250 mm, respectively. The nominal thickness of the layer was 0.2 mm. The ends of the coupons were placed in between two steel tabs with a length of 50 mm at each end. The steel tabs and GFRP sheets were bonded by using epoxy. These steel tabs were placed in between the grips of the tensile testing machine. The tensile coupon tests were conducted at the Middle East Technical University, Ankara. The tensile test results of four coupon samples were provided in Table 3.6 and Figure 3.3. The average values of the nominal thickness (t_f), ultimate tensile strength (σ_u), rupture strain capacity (ϵ_{fu}) and modulus of elasticity of GFRP fabrics were 0.2 mm, 982.6 MPa, 2 % and 50250 MPa, respectively.

Table 3.6 Coupon test results

Specimen	Tensile Strength (MPa)	Avg. Tensile Strength (MPa)	Rupture Strain Capacity (%)	Avg. Rupture Strain Capacity (%)	Modulus of Elasticity (MPa)	Avg. Modulus of Elasticity (MPa)
GFRP-1	934.4	982.6	1.97	2.00	50000	50250
GFRP-2	1020.8		2.00		54000	
GFRP-3	1244.4		2.12		51500	
GFRP-4	730.9		1.66		45500	

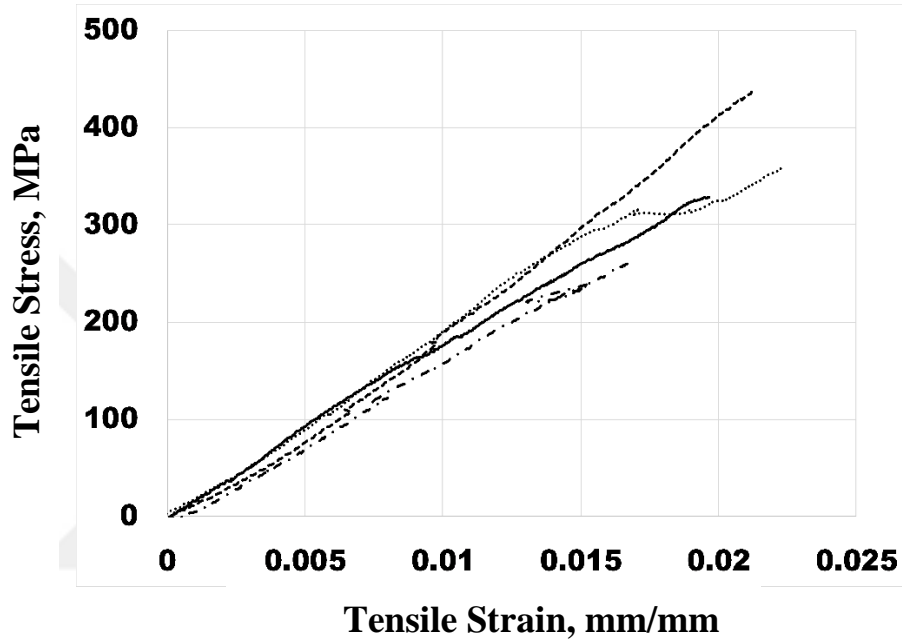


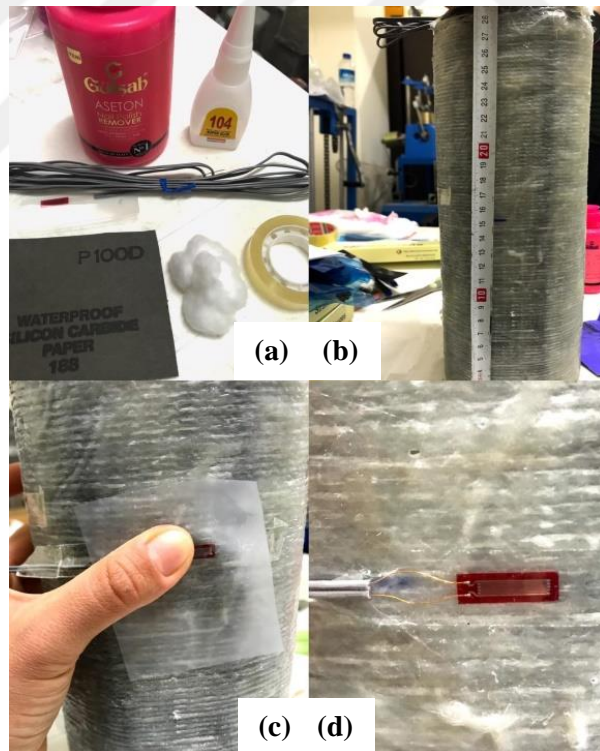
Figure 3.3. Stress-strain diagram of coupon test results

3.4. Test Setup

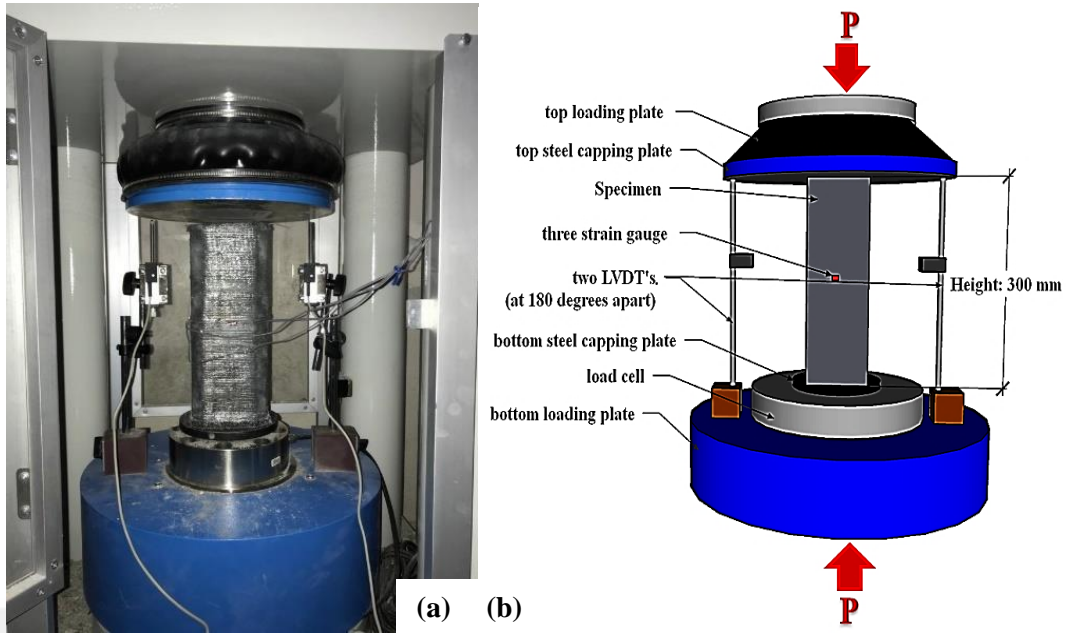
All concrete specimens were tested under monotonic axial loading (Picture 3.9). The axial load capacity of the device used for monotonic compressive loading is 3000 kN. A separate load cell with an axial load capacity of 600 kN is placed under the specimens. Thus, the ultimate load capacity of the test setup was determined by the load cell. Specimens are positioned on a high-strength circular steel disk with a diameter of 150 mm. The axial load is applied only to the core concrete which ensured by the total thickness of the unconfined region and high-strength mortar at both ends of the specimen. Therefore, the formation of axial stresses on the confining jacket was prevented and the GFRP layers were restrained only along the hoop direction.

Strain gauges with a gauge length of 10 mm were installed to measure the strains of the GFRP confined specimens before the testing phase. The area where the strain gauges will be attached was leveled with the help of sandpaper (Picture 3.8.a.). Three strain gauges were placed at the mid-height of the specimens on three surfaces (Picture 3.8.b). One surface where overlapping exists was left without strain gauge. After the leveled area was cleaned with acetone, the strain gauges were attached to the surface (Picture 3.8.c-d).

The compression tests were conducted by applying constant stress (0.25 MPa/s) based loading according to ASTM C39/C39M-20 (2020). Consequently, the axial loading rate was 2.8 and 4.4 kN/s for the specimens with square and circular sections, respectively. Two linear variable displacement transducers (LVDTs) were placed between loading and supporting plates (Picture 3.9). LVDTs were separated by 180 degrees around the specimen and fixed to the supporting plate with the help of magnetic bases. The axial deformations of the specimens during the tests were recorded by means of these LVDTs.



Picture 3.8. Strain gauge application stages



Picture 3.9. Compressive test system: (a) Test setup and (b) schematic illustration

4. TEST RESULTS

In this section, the test results obtained under monotonic compressive loading are given. The observed failure modes for different test groups are attempted to be explained first. Then, the test data is given in graphics and tables. The ultimate axial strength of unconfined (f_{co}) and confined (f_{cc}) specimens, the axial strain capacity of unconfined (ϵ_{co}) and confined (ϵ_{cu}) specimens, and strength- and strain-enhancement ratios (f_{cc}/f_{co} and $\epsilon_{cu}/\epsilon_{co}$, respectively) are obtained from the test results.

4.1. Failure Modes

The reference specimen that was wrapped with 2 layers of GFRP without rounded corners failed by a local rupture of the jacket between the mid-height and bottom. The rupture of the GFRP took place exactly at the corner which may show the effect of concentrated stress at the sharp edges without rounding. This situation is presented in Picture 4.1.



Picture 4.1. The failure mode of specimen, SRef-2G-NP

The specimens in the S15-1G-NP test group failed by the rupture of the jacket mostly in the mid-height at a location where overlapping does not exist. The failure of the companion polyurea-coated specimens (i.e. in the S15-1G-P test group) was also occurred in the mid-region. However, GFRP ruptures are generally localized even in a smaller area compared to the specimens without polyurea as shown in Picture 4.2. The rupture of the GFRP took place slightly away from the rounded corners in most of these specimens.



Picture 4.2. Failure modes of S15-1G-NP and S15-1G-P groups

The specimens in the S15-2G-NP and S15-2G-P test groups failed in a similar way as observed in the companion specimens with 1-layer of GFRP confinement. The failure by rupture of the GFRP jacket took place at about the mid-zone on one face. The location of the rupture was closer to the rounded edge in some of the specimens. There was no considerable difference in the rupture of the two-layers of GFRP jacket between the test groups without and with polyurea (Picture 4.3).



Picture 4.3. Failure modes of S15-2G-NP and S15-2G-P groups

Rupture was observed irregularly in the specimens with 30 mm rounded corners confined with a single layer of GFRP fabric. Unlike the specimens without polyurea, the failure zone was closer to the mid-zone in the S30-1G-P test group. The specimens after the test can be observed in Picture 4.4.



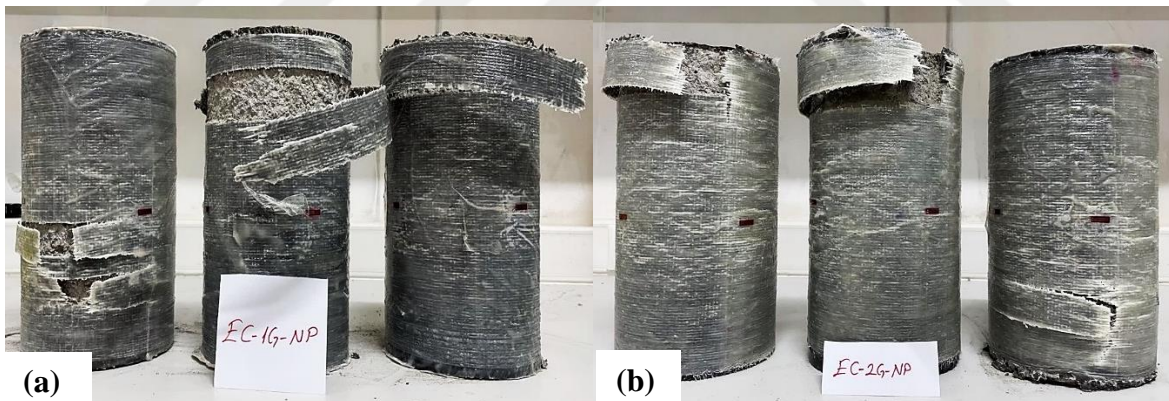
Picture 4.4. Failure modes of S30-1G-NP and S30-1G-P groups

The failure occurred by rupture of the jacket at the upper end of the specimens in the S30-2G-NP test group. The rupture took place in a much larger area compared to the previous test groups. Besides, the failure was more sudden and explosive. On the other hand, the failure occurred in the lower mid-region of the specimens coated with polyurea, unlike the companion specimens without polyurea. The rupture was less sudden and less explosive in the specimens with polyurea. Besides, the failure took place on a considerably smaller area (Picture 4.5). Also, it should be noted that the polyurea layer ruptured together with the GFRP jacket as stated by Akin et al. (2020). According to the test results, failure was observed in all specimens with polyurea as stated by Akin et al.



Picture 4.5. Failure modes of S30-2G-NP and S30-2G-P groups

The specimens with circular cross-sections failed mostly at the top portion of the specimens. However, it was closer to the mid-height in two of the specimens, even it was near the bottom end in the last specimen (Picture 4.6). Similar to the specimens in the S30-2G test groups (with or without polyurea), the failure was more severe and took place on a larger area in comparison to the previous test groups.



Picture 4.6. (a) Failure modes of EC-1G-NP group, (b) Failure modes of EC-1G-P group

4.2. Axial Stress-Strain Response

Stress-strain curves were obtained for all specimens under the monotonic axial loading. The axial strain values were calculated from the average of the data obtained by two LVDT's (i.e. divided by the specimen height). At the same time, the axial stress values were determined by the load per unit area of the specimens.

It should be noted that the applied confinement is assessed as sufficient or insufficient according to the slope of the second portion of the confined concrete response which takes place after about unconfined concrete strength level. If the second portion is in an ascending trend, the confinement is regarded as sufficient, otherwise insufficient (Lam and Teng, 2003b). The limit between these two cases may be defined as the threshold confinement where the slope of the second portion is zero (i.e. horizontal second portion). This is illustrated in Figure 4.1 which also provides the definitions that is required in the following sections.

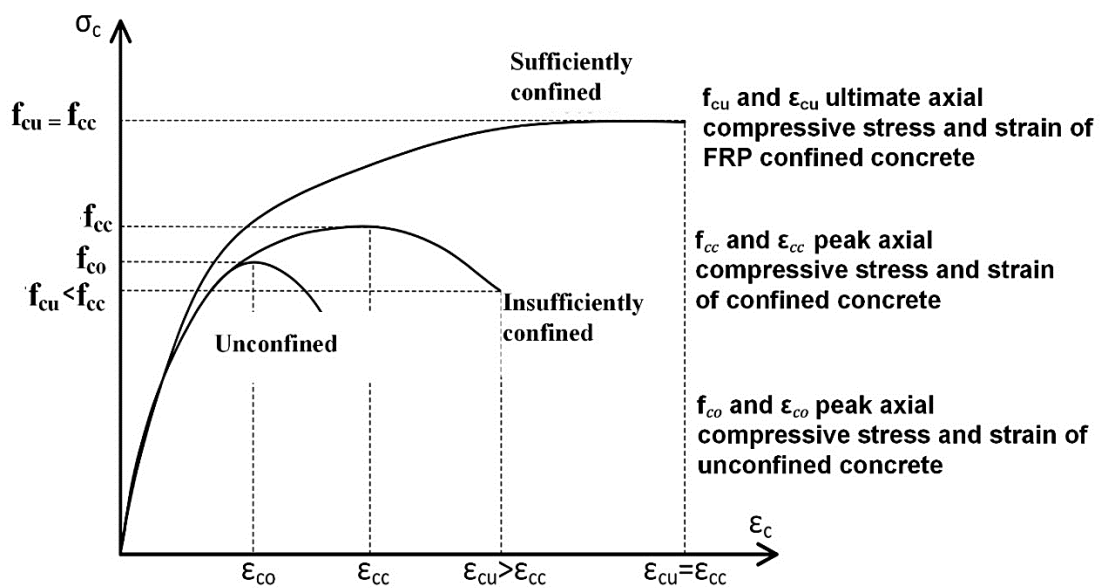


Figure 4.1. Theoretical stress-strain curves for confined and unconfined concrete

The test results of unconfined specimens provided an average compressive strength (f_{co}) of 9.6 MPa at a strain (ϵ_{co}) of approximately 0.0024 as seen in Figure 4.2.

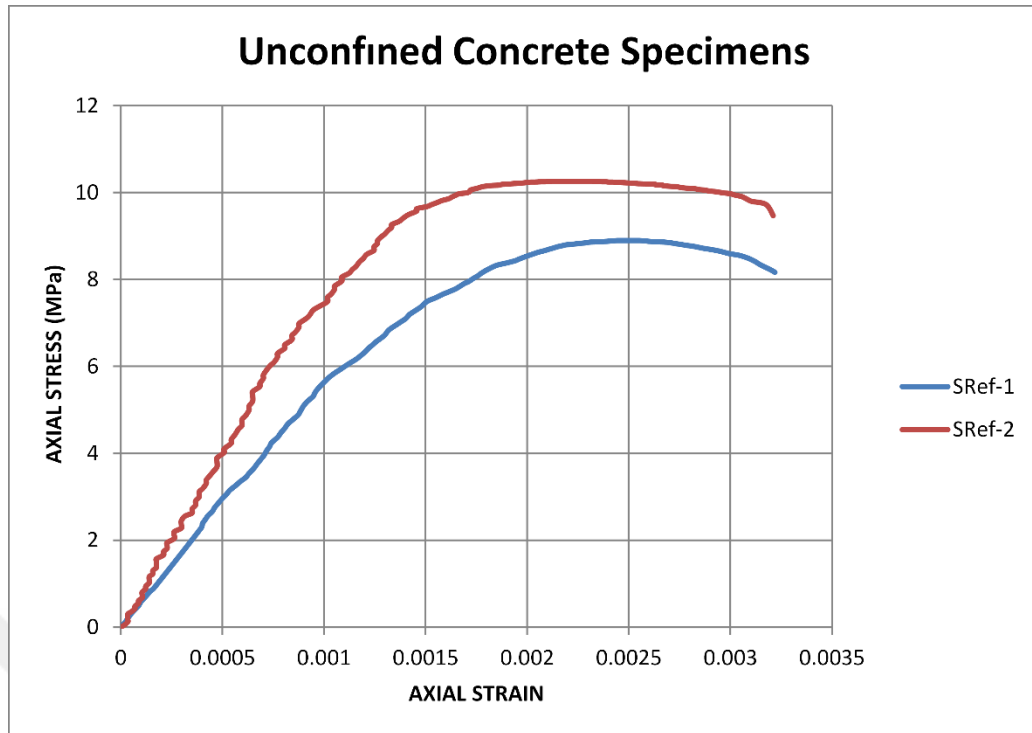


Figure 4.2. Stress-strain curve for unconfined concrete

As shown in Figure 4.3, the second portion of the axial stress-strain diagram is almost horizontal for the specimen SRef-2G-NP. When this axial stress-strain curve is assessed in accordance with Figure 4.1, it may be stated that two-layers of GFRP is a threshold confinement thickness for the specimen geometry (without corner rounding) and concrete strength considered here.

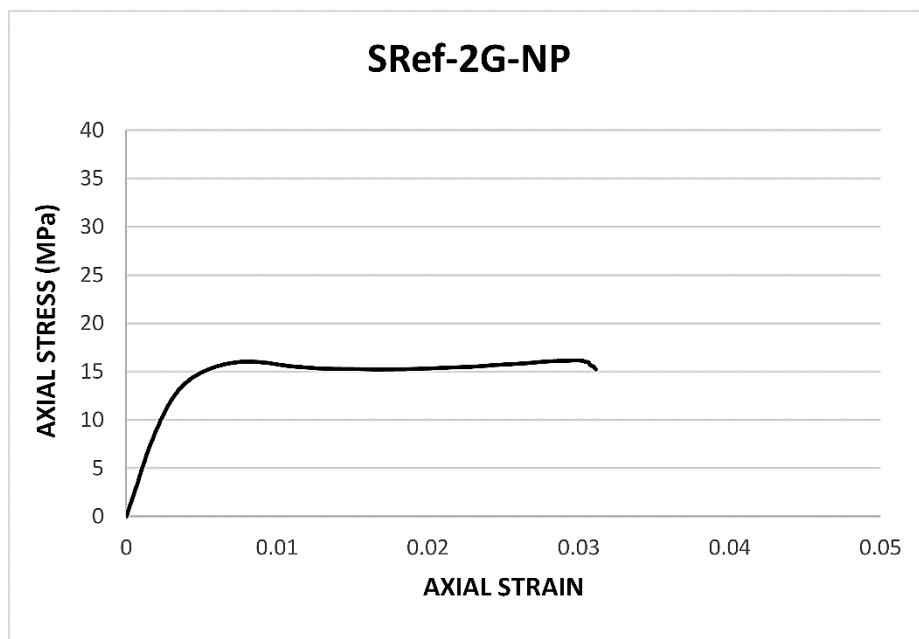


Figure 4.3. Stress-strain curve for the specimen SRef-2G-NP

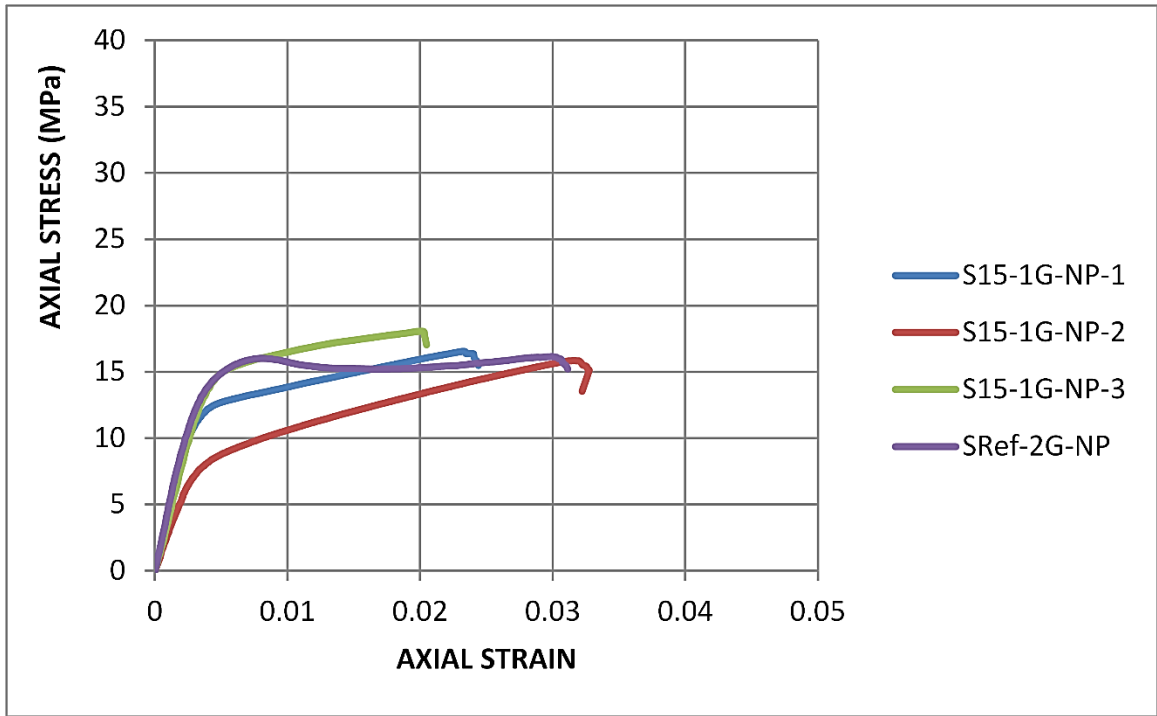


Figure 4.4. Stress-strain curves for group of S15-1G-NP

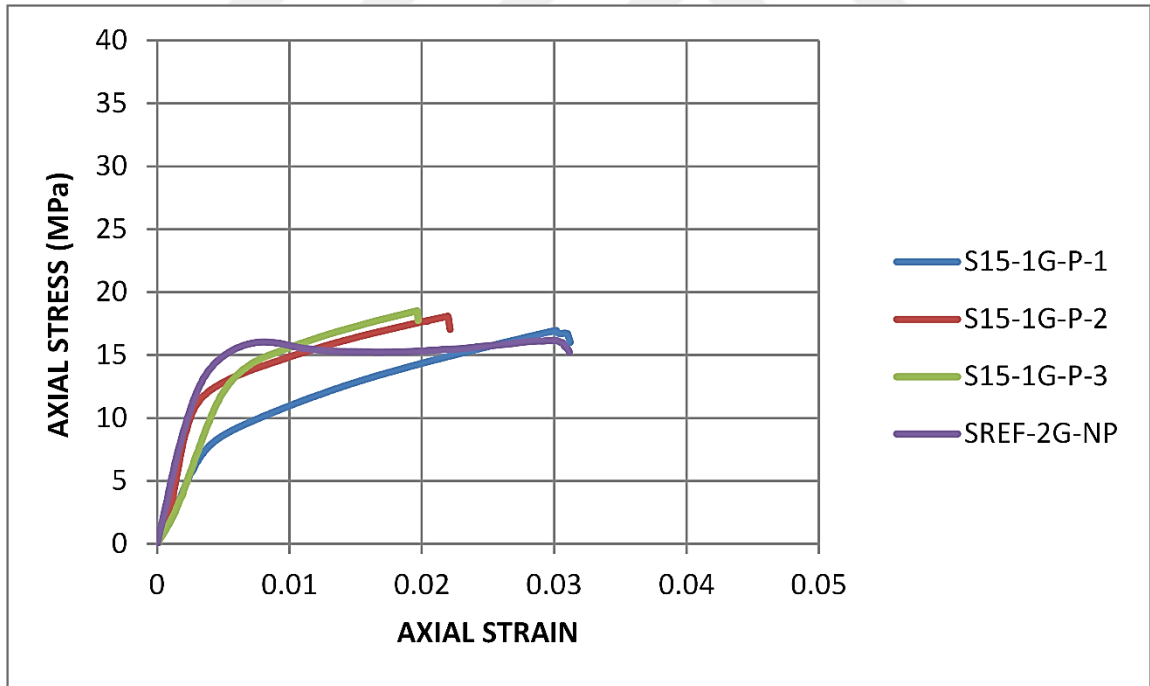


Figure 4.5. Stress-strain curves for group of S15-1G-P

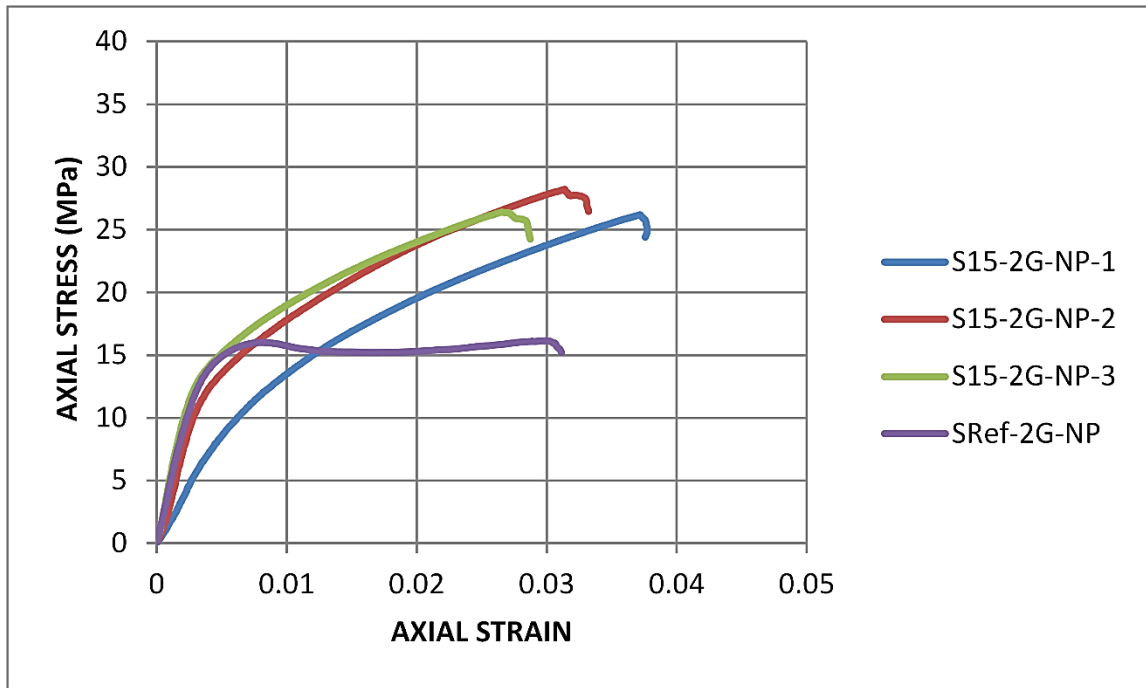


Figure 4.6. Stress-strain curves for group of S15-2G-NP

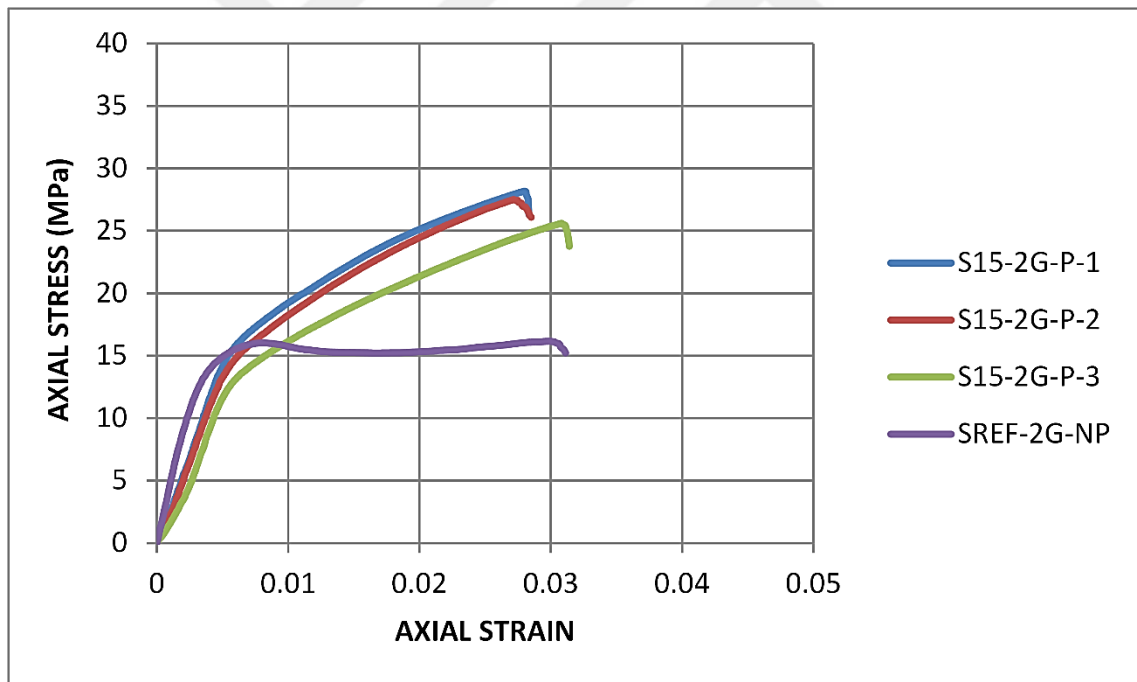


Figure 4.7. Stress-strain curves for group of S15-2G-P

In Figure 4.4, 4.5, 4.6 and 4.7, the axial stress-strain curves are given for the specimens with 15 mm rounded corners in different test groups in comparison to the axial behavior of specimen SRef-2G-NP. These figures clearly show that rounding the sharp edges by 15 mm corner radius provided sufficient confinement with increasing trend in the second portion of the curves. In this regard, even one-layer of GFRP confined specimens with rounded corners

may be regarded as more successful compared to the specimen with sharp edges by attaining at least the same level of ultimate strength or higher. On the other hand, a similar statement cannot be done by considering the axial deformation capacity (i.e. ductility) of these specimens. The use of two-layers of GFRP confinement clearly increased the slope of the second portion and thus the confinement efficiency.

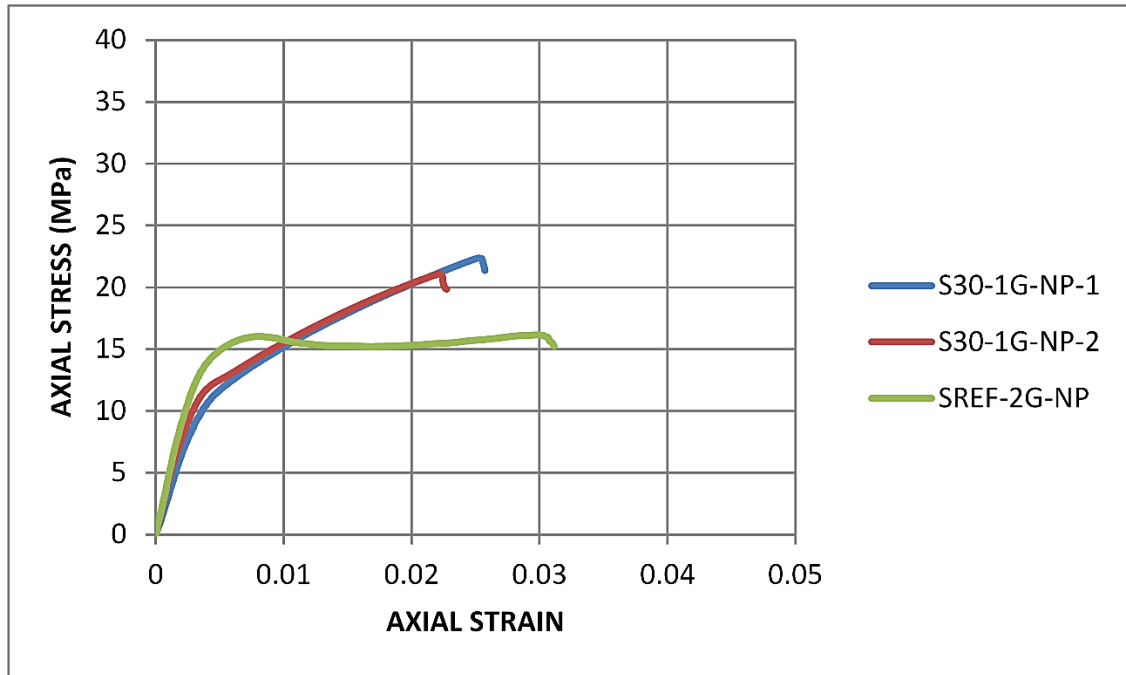


Figure 4.8. Stress-strain curves for group of S30-1G-NP

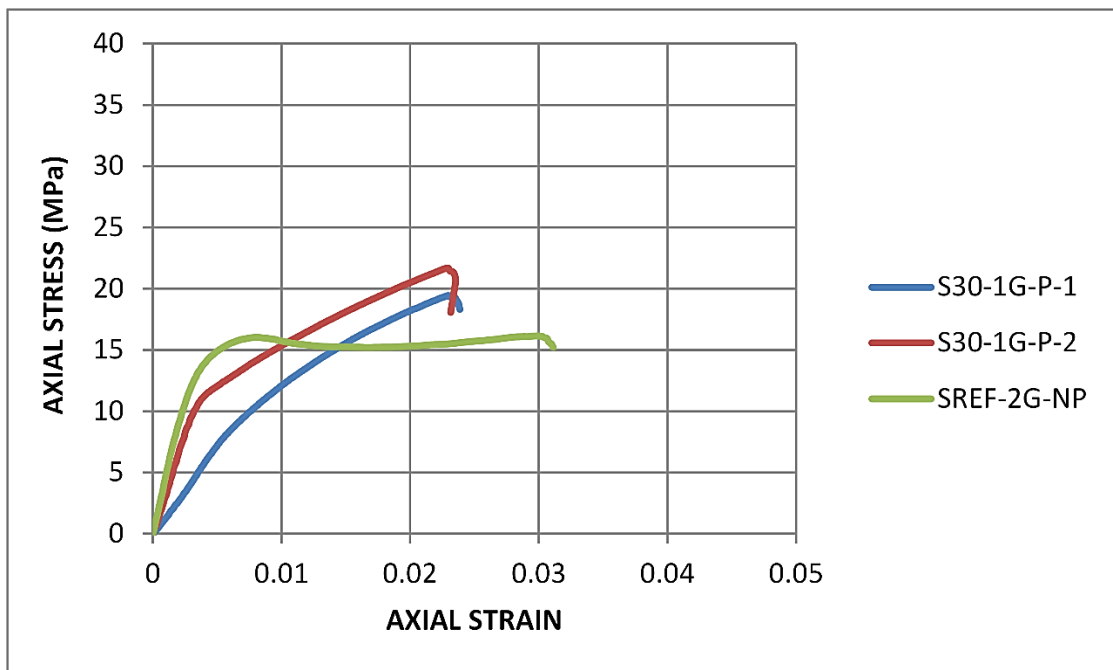


Figure 4.9. Stress-strain curves for group of S30-1G-P

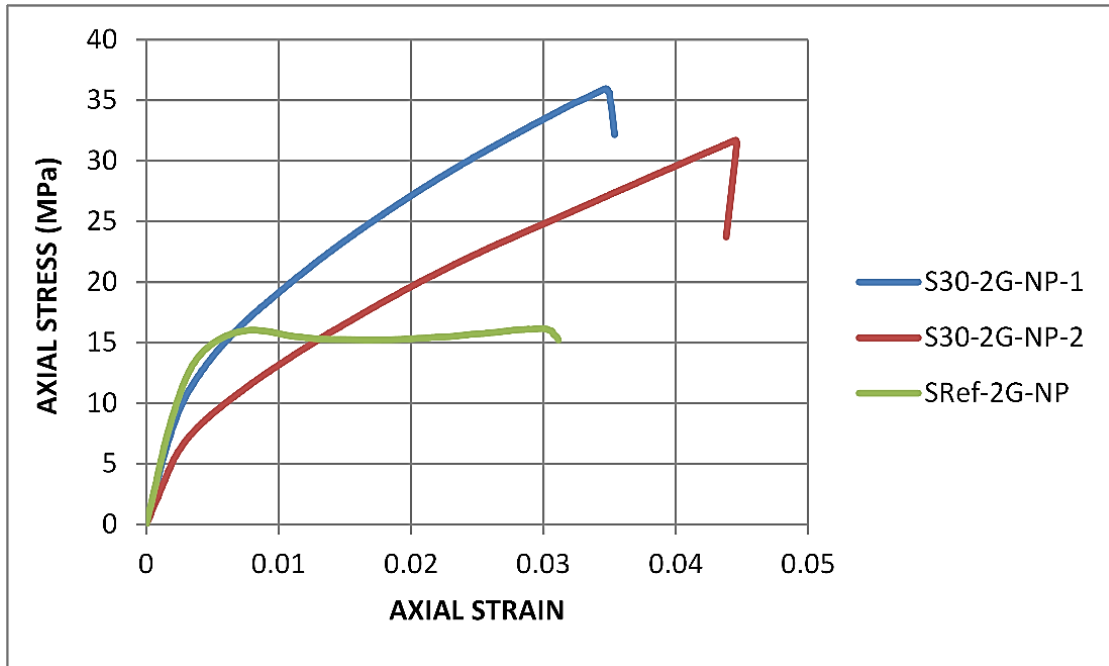


Figure 4.10. Stress-strain curves for group of S30-2G-NP

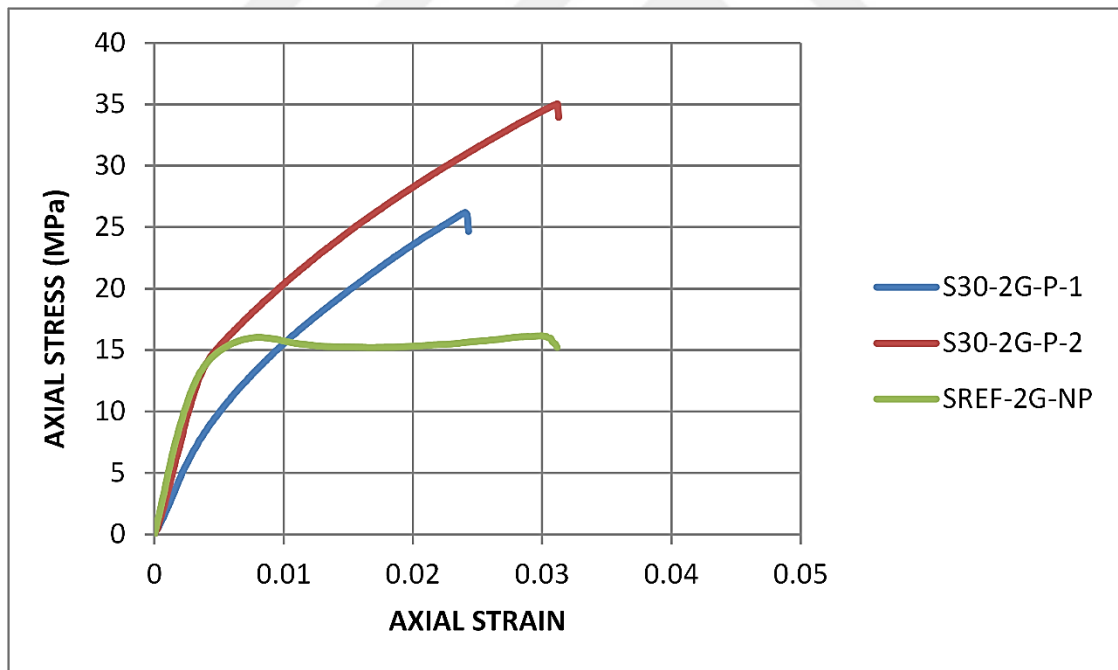


Figure 4.11. Stress-strain curves for group of S30-2G-P

In Figure 4.8, 4.9, 4.10 and 4.11, the axial stress-strain curves are given for the specimens with 30 mm rounded corners in different test groups in comparison to the axial behavior of specimen SRef-2G-NP. The results show that rounding the sharp edges further

by 30 mm resulted in a better confinement efficiency. It should be noted that no explicit effect of polyurea may be observed in Figures 4.8, 4.9, 4.10 and 4.11.

Likewise, Figures 4.12 and 4.13 show the axial stress-strain curves for the specimens with equivalent circular section with one- and two-layers of GFRP confinement, respectively. The increase in the confinement thickness increased the confinement efficiency in terms of both strength and ductility considerably.

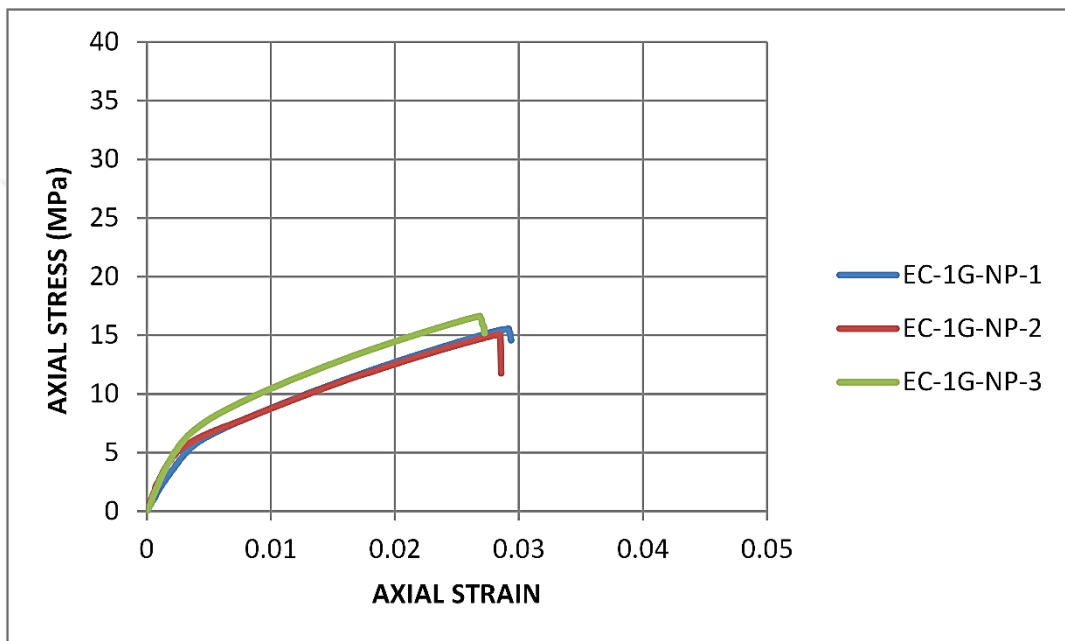


Figure 4.12. Stress-strain curves for group of EC-1G-NP

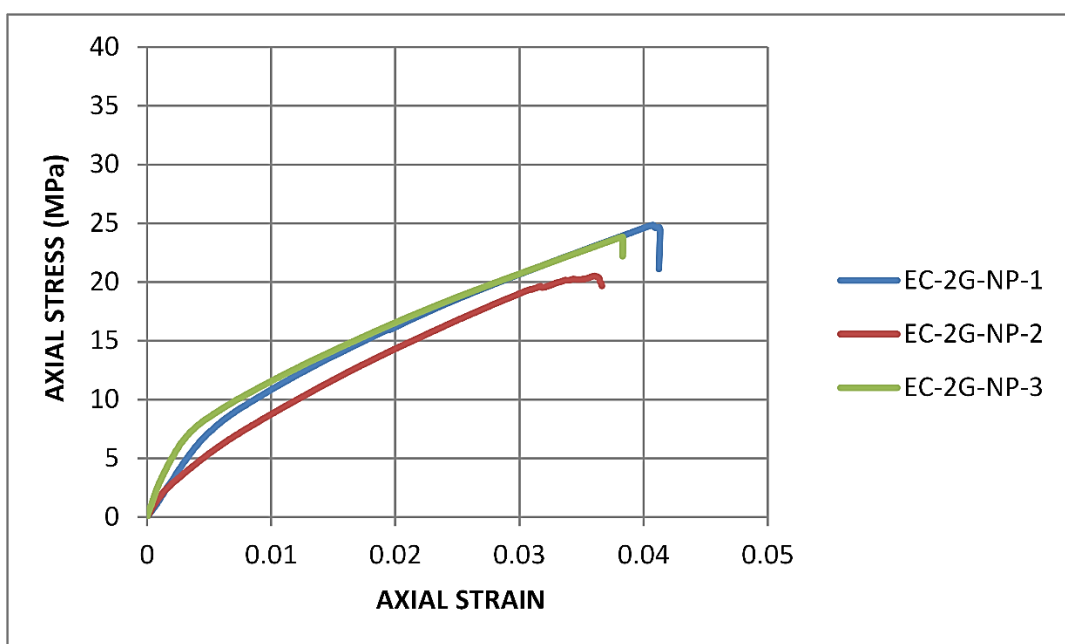


Figure 4.13. Stress-strain curves for group of EC-2G-NP

The axial stress-strain diagrams of the S15-1G-NP and S30-1G-NP groups are presented in Figure 4.14. Figure 4.15 shows the axial stress-strain diagram of the S15-1G-P and S30-1G-P groups. The axial stress-strain diagrams of the S15-2G-NP and S30-2G-NP groups are presented in Figure 4.16. Likewise, Figure 4.17 contains the axial stress-strain diagrams of the S15-2G-P and S30-2G-P groups. The comparisons according to these diagrams will be stated in the discussion section.

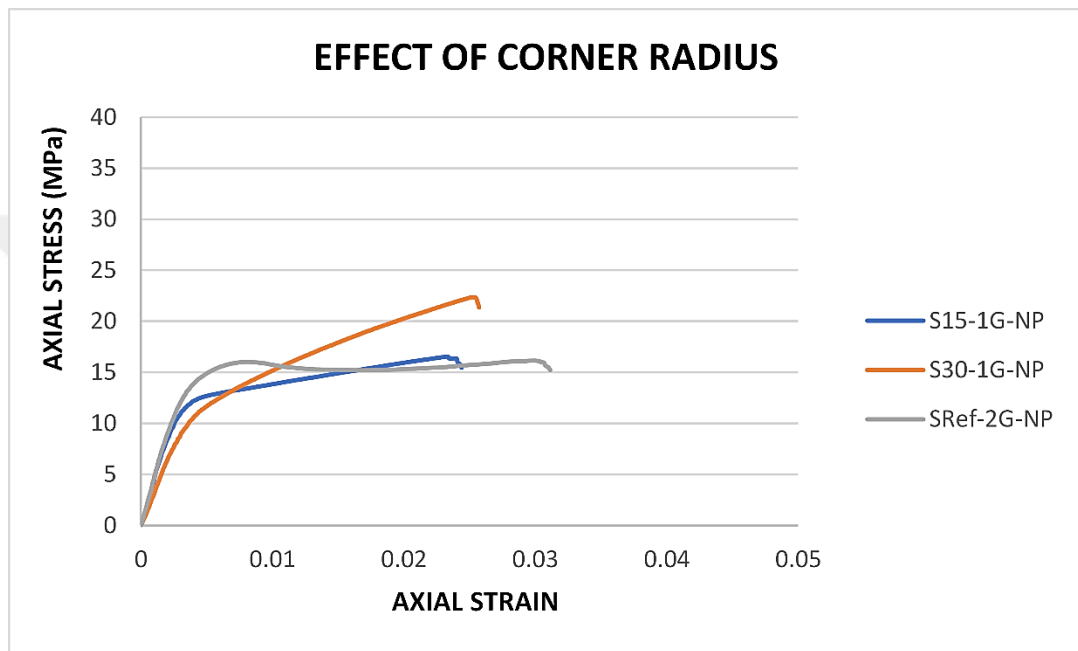


Figure 4.14. Axial stress-strain diagram of comparison between S15-1G-NP and S30-1G-NP

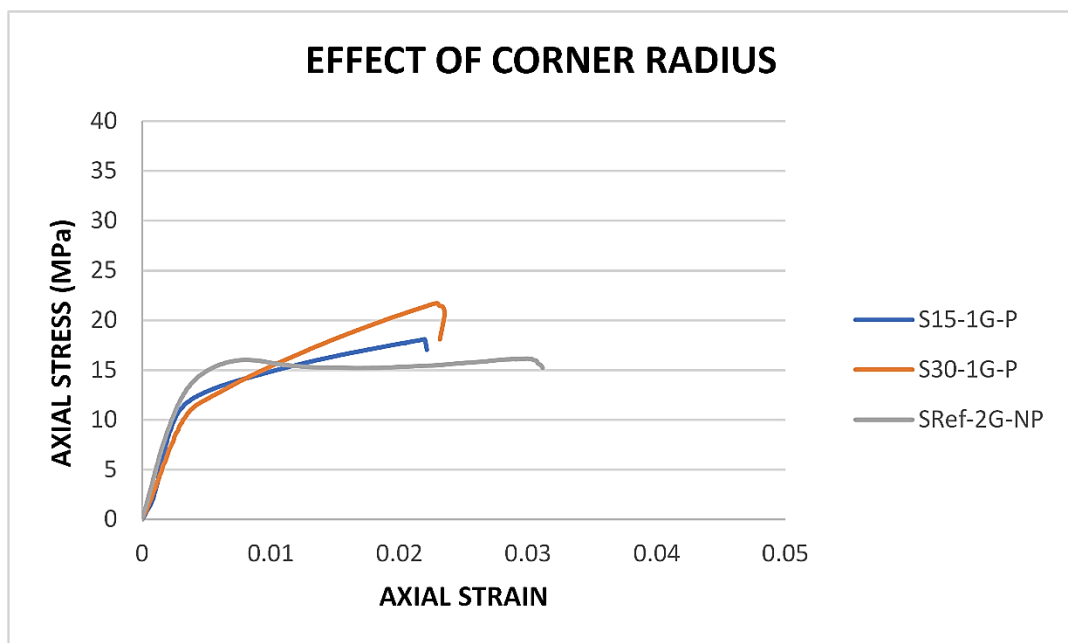


Figure 4.15. Axial stress-strain diagram of comparison between S15-1G-P and S30-1G-P

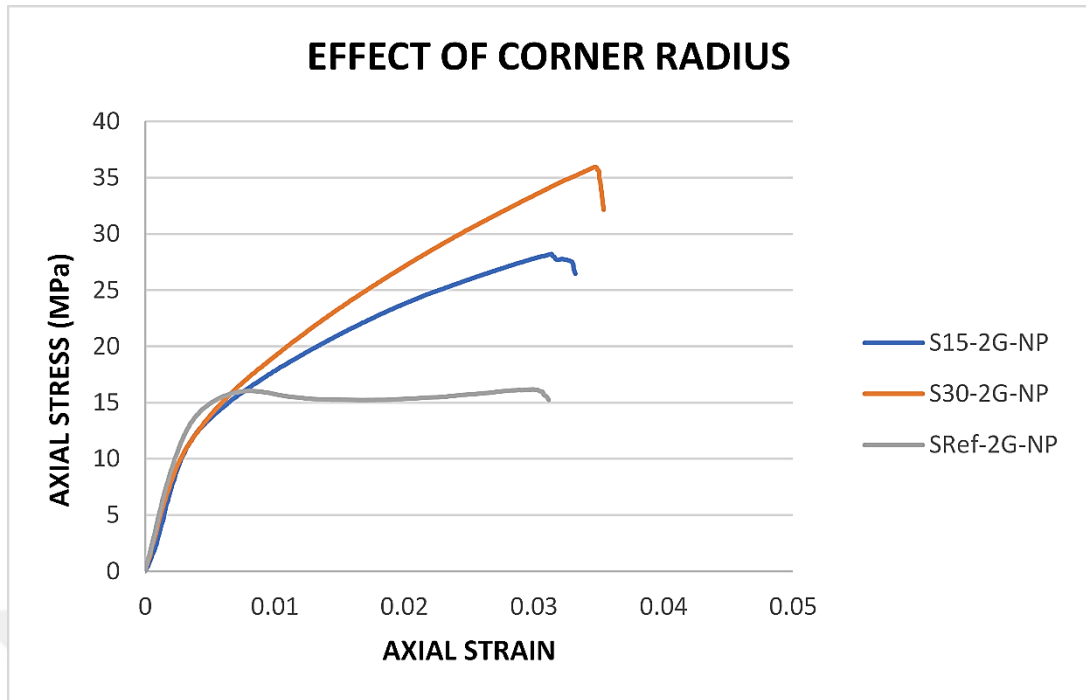


Figure 4.16. Axial stress-strain diagram of comparison between S15-2G-NP and S30-2G-NP

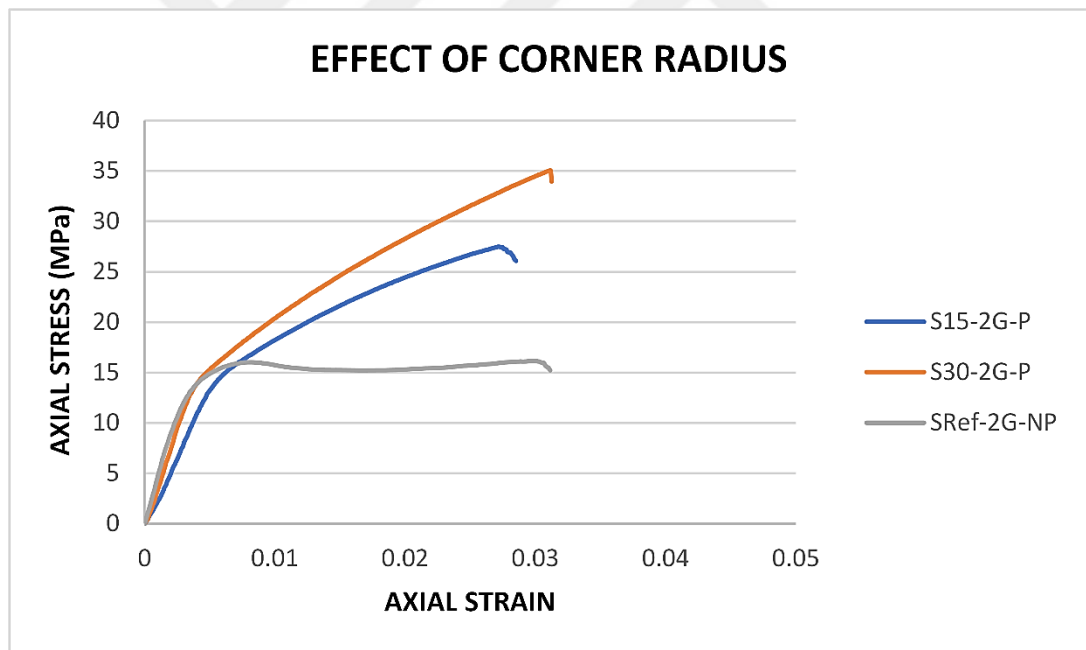


Figure 4.17. Axial stress-strain diagram of comparison between S15-2G-P and S30-2G-P

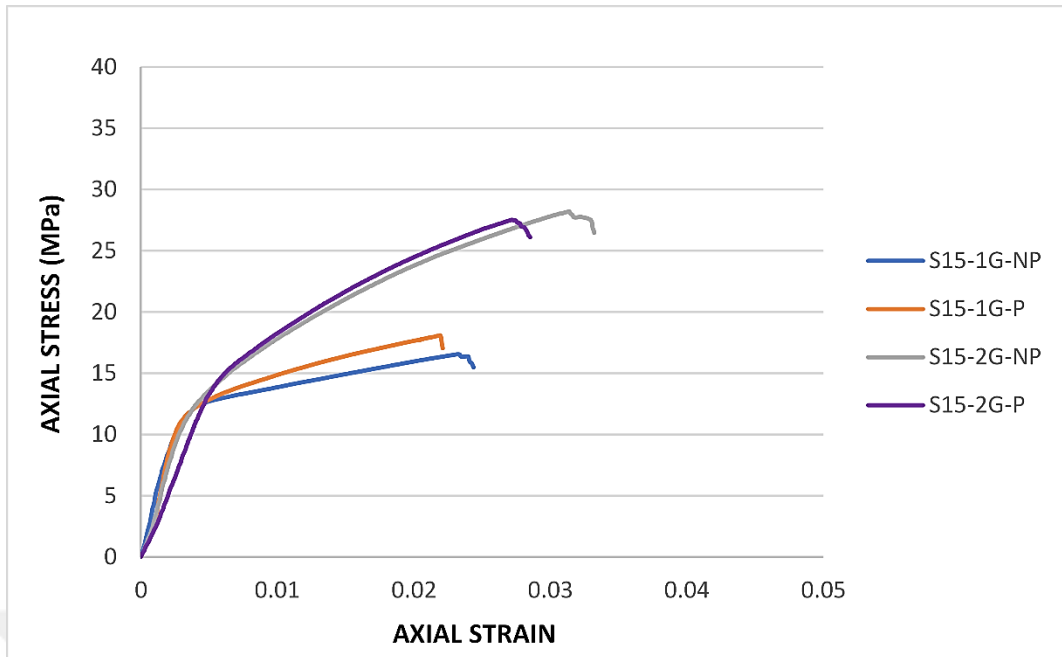


Figure 4.18. Axial stress-strain diagram of S15 group

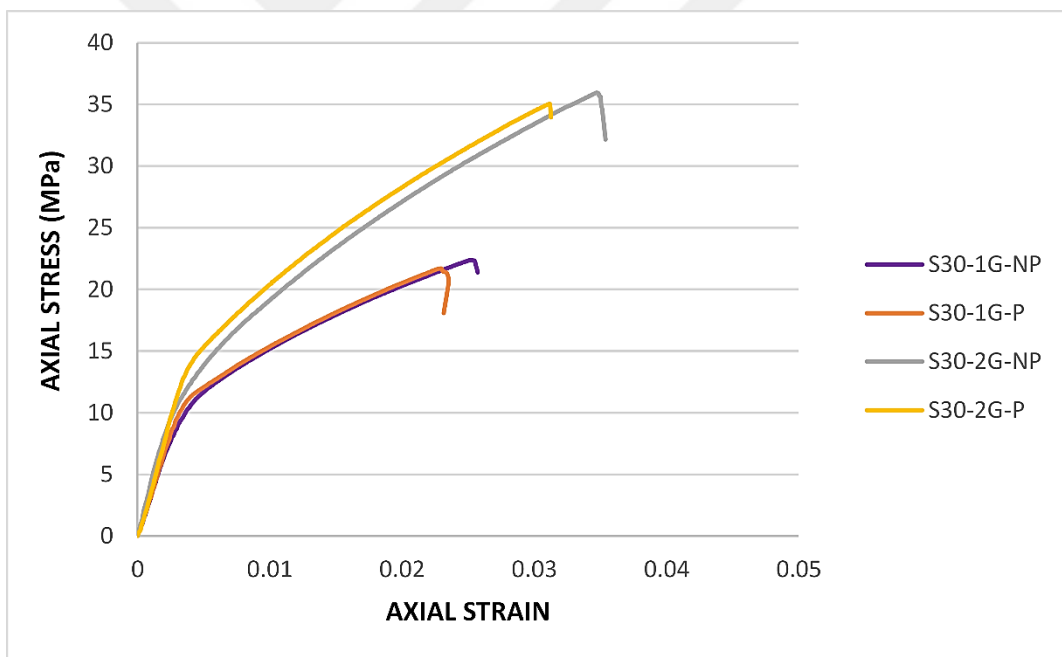


Figure 4.19. Axial stress-strain diagram of S30 group

Figure 4.18 shows the axial stress-strain diagrams for the S15 group, while Figure 4.19 shows the axial stress-strain diagrams for the S30 group. The comparisons according to these diagrams will be stated in the discussion section (i.e. examining the polyurea effect and the effect of the number of layers).

4.3. Test Results

The ultimate stress (f_{co} for the unconfined and f_{cc} for the confined specimens) and strain (ϵ_{cu} for the confined specimens) values were determined separately for each specimen. Besides, the strain corresponding to the ultimate strength (ϵ_{co}) was determined in the case of unconfined specimens. On the other hand, in the GFRP confined specimens, the ultimate lateral strain values measured by the strain gauges were obtained for each specimen. In addition, strength- and strain-enhancement ratios (f_{cc}/f_{co} and $\epsilon_{cu}/\epsilon_{co}$, respectively) are estimated for each specimen. All of these information are provided in Table 4.1.

It is known that the ultimate hoop rupture strain of the FRP used for the confinement remains lower than the ultimate tensile stress specified by the manufacturer or obtained by coupon tests (Lam and Teng, 2003b; Ozbakkaloglu and Oehlers, 2008; Akin et al., 2020). Therefore, a strain reduction factor is used to calculate the ultimate tensile strain of the same composite material (Eqn. 1).

$$k_e = \frac{\epsilon_{hrup}}{\epsilon_{coupon}} \quad (1)$$

The hoop rupture strain (ϵ_{hrup}) to calculate the reduction factor (k_e) in Eqn.1 is the average of the maximum lateral (hoop) strain measured by three strain gauges during the tests. ϵ_{coupon} is the strain of the GFRP material obtained from the coupon tests shown in Table 3.6.

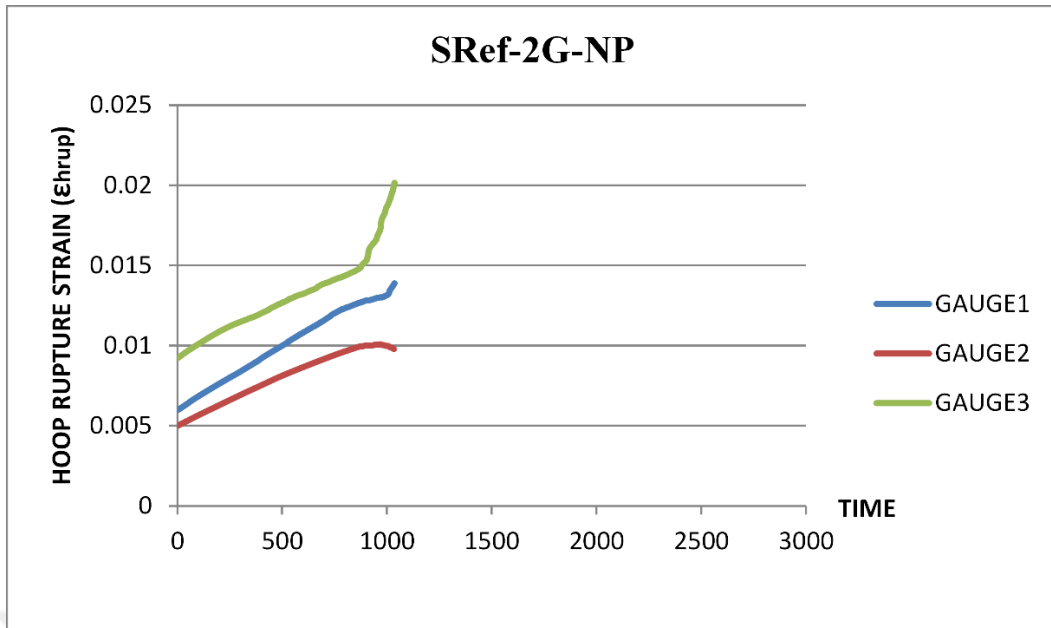


Figure 4.20. Hoop rupture strain diagram for SRef-2G-NP

Figure 4.20 shows the time-dependent hoop rupture strain diagrams of the SRef-2G-NP specimen. The hoop rupture strain diagram of the S15-1G-NP specimens is given in Figure 4.21, while the hoop rupture strain values of the S15-1G-P specimens are in Figure 4.22. The hoop rupture strain diagram of S15-2G-NP specimens is given in Figure 4.23. On the other hand, hoop rupture strain values of S15-2G-P specimens are shown in Figure 4.24.

Figure 4.25 shows the hoop rupture strain diagram of the S30-1G-NP specimens. The hoop rupture strain diagram of the S30-1G-P specimens is given in Figure 4.26. In addition, Figure 4.27 shows the hoop rupture strain diagram for S30-2G-NP specimens, while Figure 4.28 shows the hoop rupture strain diagram of S30-2G-P specimens.

The hoop rupture strain diagrams of EC-1G-NP specimens are presented in Figure 4.29. In Figure 4.30, hoop rupture strain diagrams of EC-2G-NP specimens are given. The discussions according to the hoop rupture strain graphs will be in the next section.

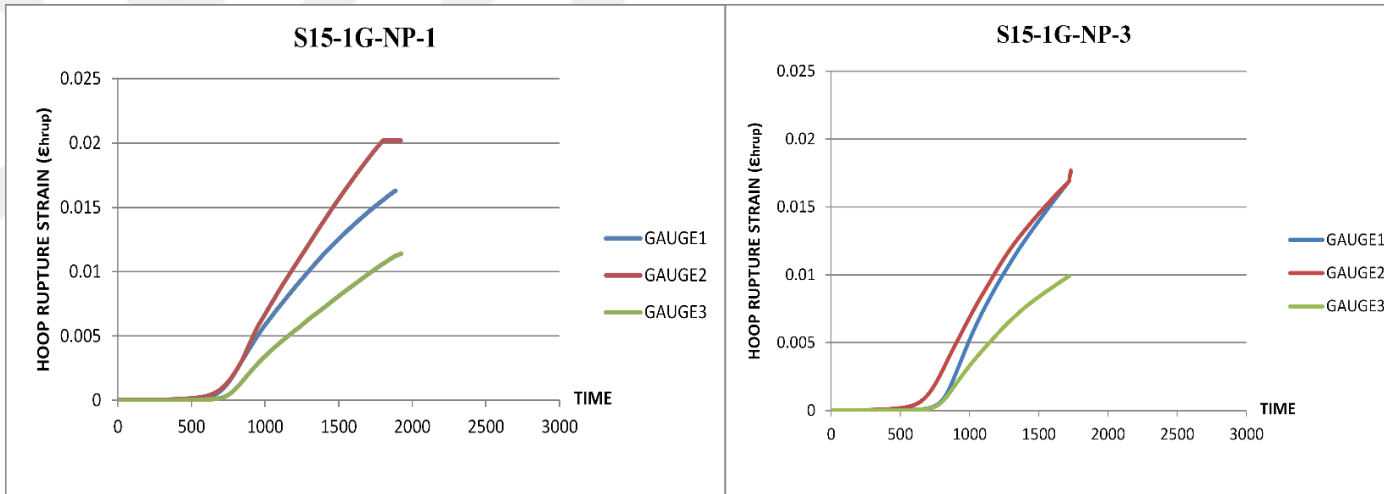


Figure 4.21. Hoop rupture strain diagram for S15-1G-NP group

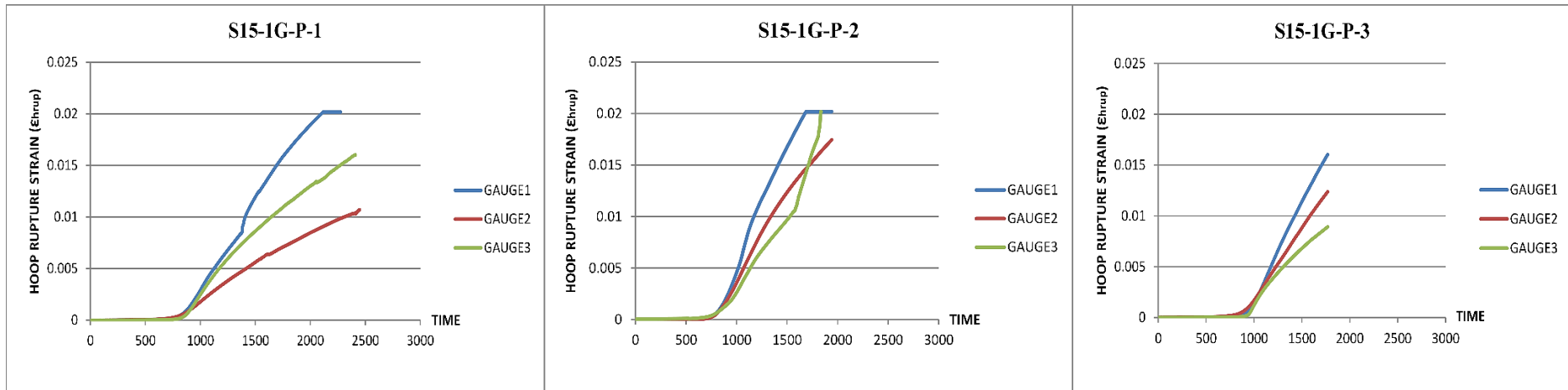


Figure 4.22. Hoop rupture strain diagram for S15-1G-P group

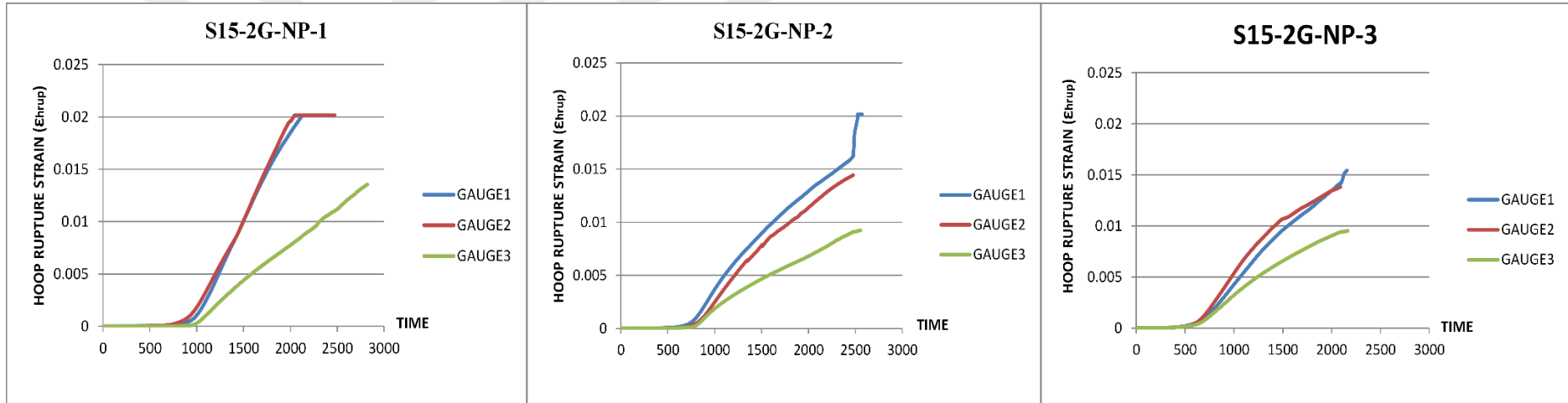


Figure 4.23. Hoop rupture strain diagram for S15-2G-NP group

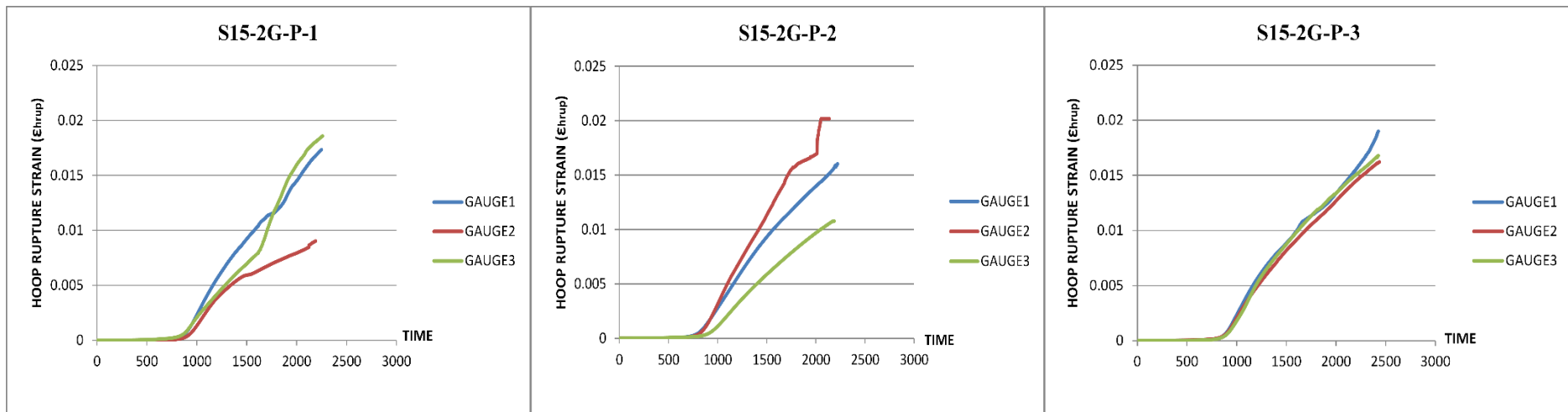


Figure 4.24. Hoop rupture strain diagram for S15-2G-P group

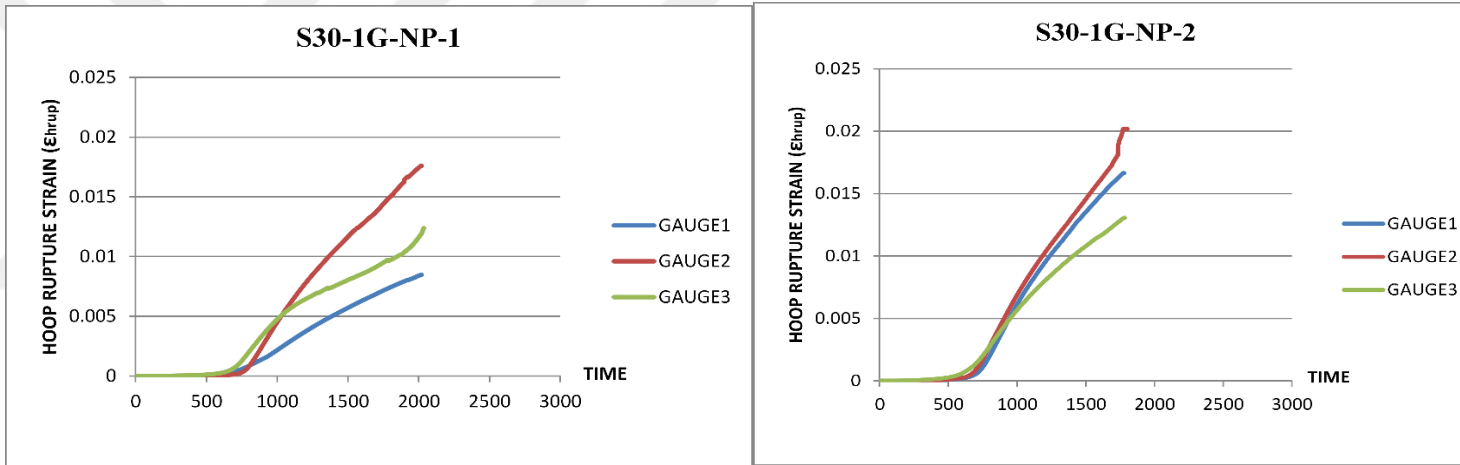


Figure 4.25. Hoop rupture strain diagram for S30-1G-NP group

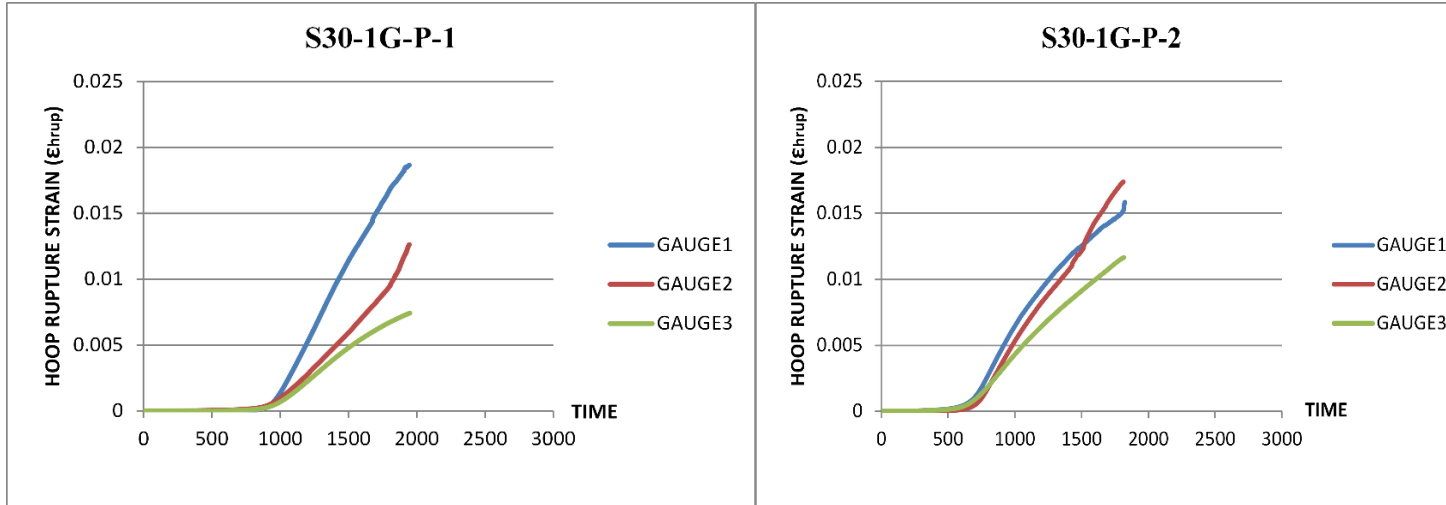


Figure 4.26. Hoop rupture strain diagram for S30-1G-P group

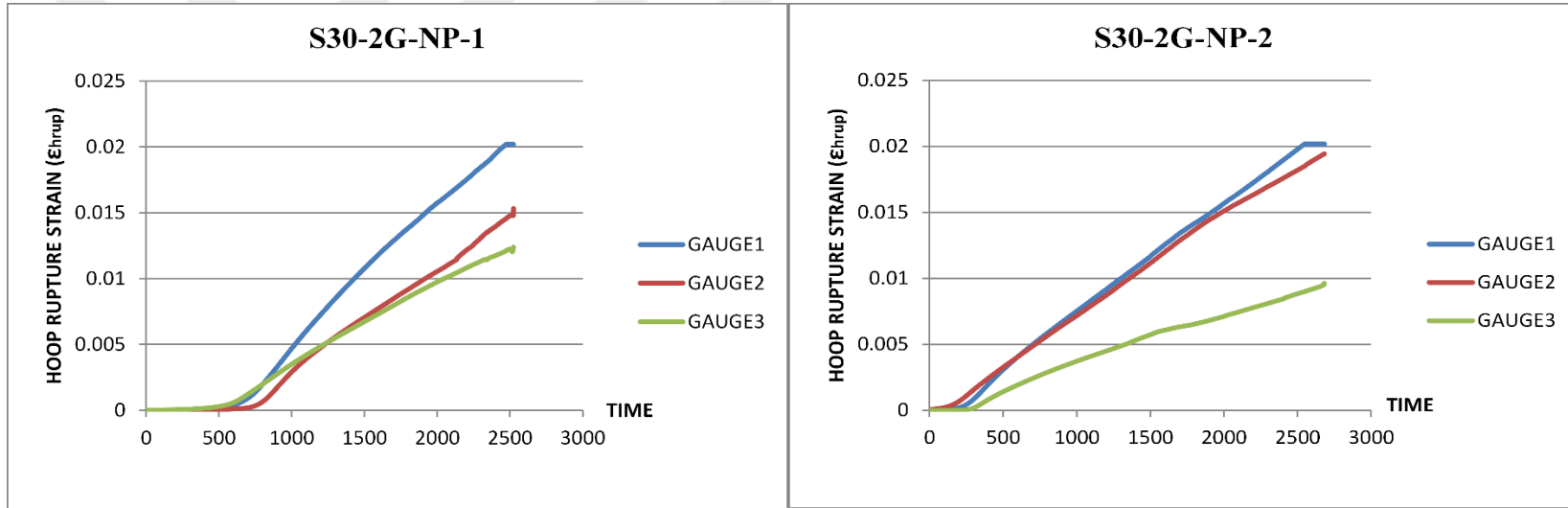


Figure 4.27. Hoop rupture strain diagram for S30-2G-NP group

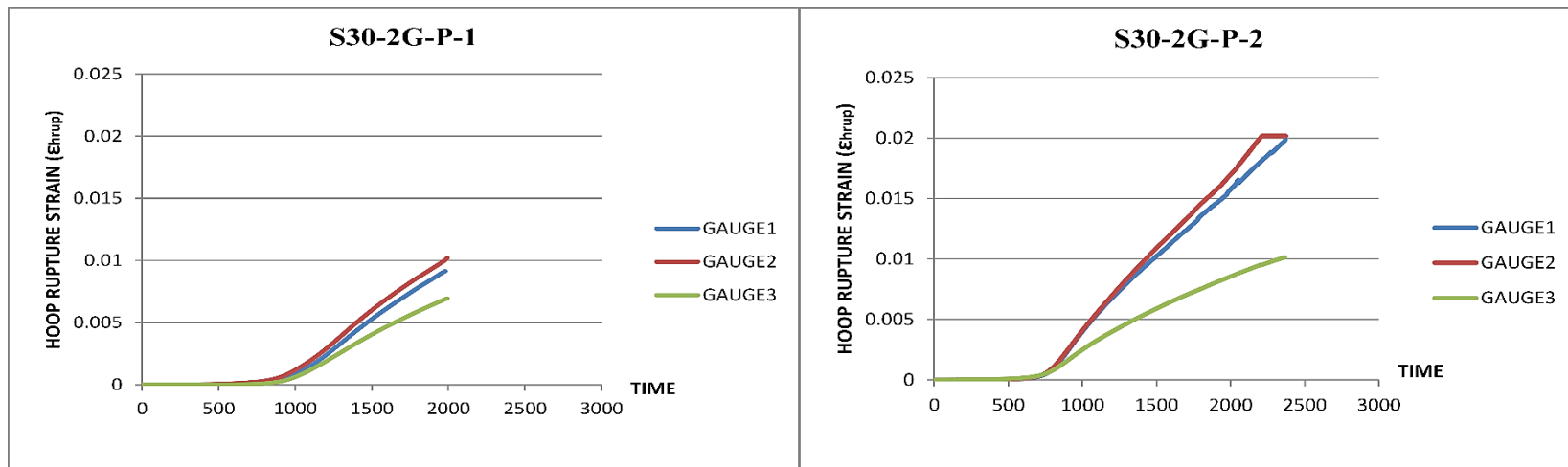


Figure 4.28. Hoop rupture strain diagram for S30-2G-P group

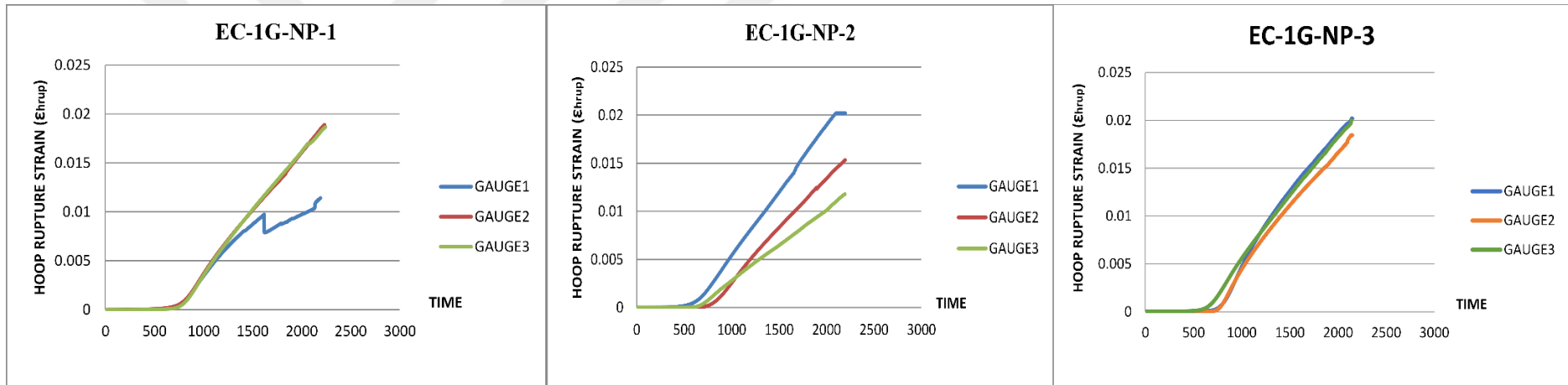


Figure 4.29. Hoop rupture strain diagram for EC-1G-NP group

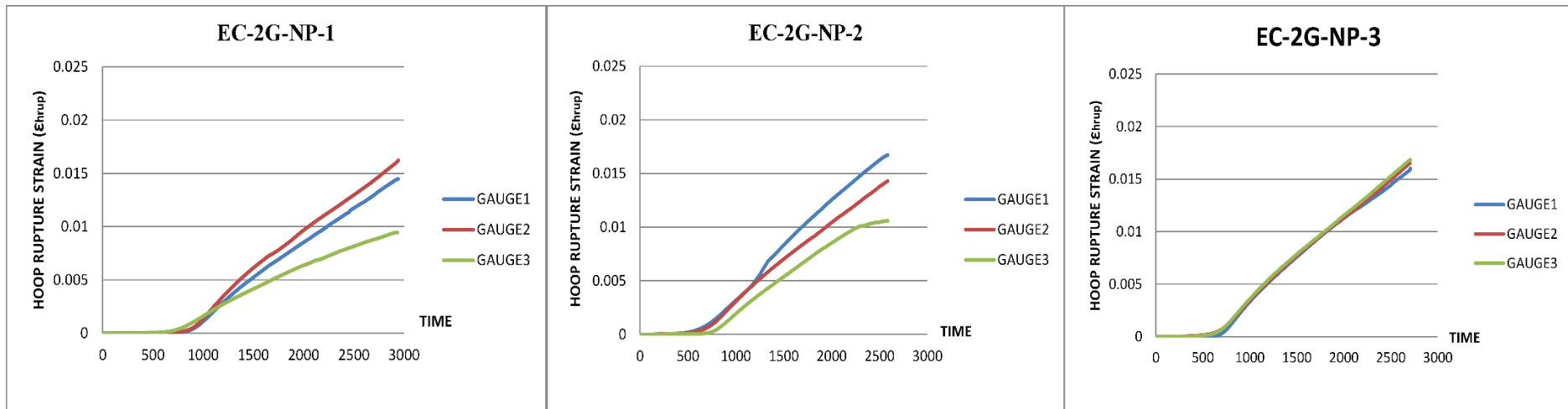


Figure 4.30. Hoop rupture strain diagram for EC-2G-NP group

Table 4.1. The test results

GROUP	Specimen	f_{cc}	Average (f_{cc})	ϵ_{cu}	Average (ϵ_{cu})	f_{cc}/f_{co}	Average (f_{cc}/f_{co})	$\epsilon_{cu}/\epsilon_{co}$	Average ($\epsilon_{cu}/\epsilon_{co}$)	ϵ_{hrup}	Average (ϵ_{hrup})	k_e ($\epsilon_{hrup}/\epsilon_{coupon}$)	Average k_e
SRef (Unconfined)	1	8.9	9.6	0.0025	0.0024	1	-	1	-	-	-	-	-
	2	10.3		0.0023									
SRef-2G-NP	1	16.2	16.2	0.03	0.03	1.68	1.68	12.50	12.50	0.015	0.015	0.75	0.75
S15-1G-NP	1	16.5	16.8	0.0233	0.0250	1.72	1.75	9.71	10.42	0.016	0.016	0.8	0.78
	2	15.9		0.0317		1.65		13.21		NA ⁽¹⁾		NA	
	3	18.1		0.02		1.88		8.33		0.015		0.75	
S15-1G-P	1	17.0	17.8	0.0302	0.0241	1.77	1.86	12.58	10.03	0.016	0.016	0.8	0.78
	2	18.1		0.022		1.88		9.17		0.019		0.95	
	3	18.5		0.02		1.93		8.33		0.012		0.6	
S15-2G-NP	1	26.2	26.9	0.0372	0.0317	2.73	2.81	15.50	13.21	0.018	0.015	0.9	0.77
	2	28.2		0.0314		2.94		13.08		0.015		0.75	
	3	26.4		0.0265		2.75		11.04		0.013		0.65	
S15-2G-P	1	28.2	27.1	0.028	0.0287	2.93	2.82	11.67	11.94	0.015	0.016	0.75	0.80
	2	27.5		0.0272		2.87		11.33		0.016		0.8	
	3	25.6		0.0308		2.67		12.83		0.017		0.85	
S30-1G-NP	1	22.4	21.7	0.0253	0.0238	2.33	2.26	10.54	9.90	0.013	0.015	0.65	0.75
	2	21.1		0.0222		2.20		9.25		0.017		0.85	
S30-1G-P	1	19.4	20.6	0.023	0.0230	2.03	2.14	9.58	9.58	0.013	0.013	0.65	0.63
	2	21.7		0.023		2.26		9.58		0.012		0.6	
S30-2G-NP	1	35.9	33.8	0.0347	0.0396	3.74	3.52	14.46	16.50	0.016	0.016	0.8	0.80
	2	31.7		0.0445		3.30		18.54		0.016		0.8	
S30-2G-P	1	26.2	30.6	0.024	0.0276	2.73	3.19	10.00	11.48	0.0087	0.014	0.435	0.72
	2	35.1		0.0311		3.65		12.96		0.02		1	
EC-1G-NP	1	15.6	15.8	0.0292	0.0282	1.62	1.64	12.17	11.75	0.016	0.017	0.8	0.87
	2	15.1		0.0285		1.57		11.88		0.016		0.8	
	3	16.6		0.0269		1.73		11.21		0.02		1	
EC-2G-NP	1	24.8	23.1	0.041	0.0383	2.59	2.40	17.08	15.97	0.013	0.014	0.65	0.72
	2	20.5		0.036		2.14		15.00		0.014		0.7	
	3	23.8		0.038		2.48		15.83		0.016		0.8	

⁽¹⁾ The rupture strain data is not available due to a technical problem that occurred during the test of this specimen

5. MODEL PREDICTIONS

Many design-oriented models estimate the axial compressive strength and ultimate axial strain (i.e. ultimate conditions) of the square/rectangular concrete columns confined by the FRP materials. Some of these models are provided by Fardis and Khalili (1982), Saadatmanesh et al. (1994), Miyauchi et al. (1997), ACI 440 (2002), Lam and Teng (2003b), Challal et al. (2003), Koksai and Doran (2009). Among these models, Lam and Teng (2003b) model for the rectangular/square sections is known to predict the ultimate conditions close to the experimental results (Toy, 2008). Therefore, Lam and Teng (2003b) model was chosen for comparison with the experimental results.

5.1. Modeling for FRP Confined Circular Cross Sections

The equations suggested by Lam and Teng (2003a) model to calculate the ultimate axial strength and strain capacity of the FRP confined circular concrete are given.

Firstly, the confining pressure (f_{lu}) must be defined as given in Eqn.2.

$$f_{lu} = \frac{2 \cdot t_f \cdot E_{frp} \cdot \epsilon_{hrup}}{D} \quad (2)$$

In Eqn.2, E_{frp} is the modulus of elasticity of the composite material (i.e. provided as 50250 MPa in Table 3.6); t_f is the thickness of the layer (i.e. 0.2 mm) which should be multiplied by the number of layers in multilayer confinement; ϵ_{hrup} is the hoop rupture strain attained during the tests (i.e. given in Table 4.1 for each specimen) ; D is the diameter of specimens with circular section.

$$\frac{f_{cc}}{f_{co}} = 1 + k_1 \frac{f_{lu}}{f_{co}} \quad (3)$$

The strength enhancement ratio (f_{cc}/f_{co}) is calculated by using Eqn. 3 for the FRP confined circular cross-sections. The bare concrete strength, f_{co} , is given in Table 4.1 (i.e. 9.6 MPa). In Eqn.3, the confinement effectiveness coefficient, k_1 is the strength-enhancement coefficient which is taken as 3.3 (i.e. a constant value) by Lam and Teng (2003a).

The strain enhancement ratio ($\epsilon_{cu}/\epsilon_{co}$) is calculated by using Eqn. 4 for the FRP confined circular cross-section.

$$\frac{\epsilon_{cu}}{\epsilon_{co}} = 1.75 + k_2 \cdot \left(\frac{f_{lu}}{f_{co}} \right) \cdot \left(\frac{\epsilon_{hrup}}{\epsilon_{co}} \right)^{0.45} \quad (4)$$

In Eqn.4, the strain-enhancement coefficient k_2 is taken as a constant value that equals to 12 by Lam and Teng (2003a).

5.2. Modeling for FRP Confined Square Sections

The axial behavior of square sections cannot be expected to be the same as for circular sections. For square sections, the area surrounded by four parabolas that cut each edge by a tangent of 45° is considered as the effectively confined area (Figure 5.1). The Lam and Teng (2003a) model has been updated for the square and rectangular sections based on the effective confinement area in the Lam and Teng (2003b).

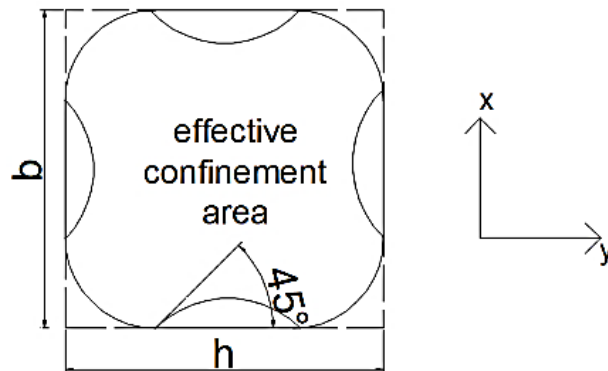


Figure 5.1. Illustration of the proposed model for FRP-confined square sections

The effective confinement area ratio A_e/A_c (i.e. ratio of the effectively confined area to the total cross-sectional area) is given in Eqn. 5.

$$\frac{A_e}{A_c} = 1 - \frac{(h-2.R_c)^2 + (b-2.R_c)^2}{3.A_g.(1-\rho_s)} \quad (5)$$

The parameters in the equation are as follows: R_c is the corner radius of the specimens where the edges are rounded; ρ_s is the ratio of the longitudinal steel rebars to the cross-sectional area; b and h are the cross-sectional dimensions; A_g is the gross area of the specimen considering the rounded corners (Eqn.6). It should be noted that ρ_s ratio is taken as zero since longitudinal reinforcement is not used while preparing the specimens in this study.

$$A_g = b.h - (4-\pi).R_c^2 \quad (6)$$

While calculating the ultimate confinement pressure, f_{lu} by using Eqn.2 for the square sections, D is calculated as the diagonal distance of the section that may be calculated by Eqn. 7.

$$D = \sqrt{b^2 + h^2} \quad (7)$$

The strength- and strain enhancement ratios are calculated by using Eqn. 8 and 9 for the FRP confined square sections.

$$\frac{f_{cc}}{f_{co}} = 1 + k_1.k_{s1} \frac{f_{lu}}{f_{co}} \quad (8)$$

$$\frac{\varepsilon_{cc}}{\varepsilon_{co}} = 1.75 + k_2.k_{s2} \left(\frac{f_{lu}}{f_{co}} \right) \left(\frac{\varepsilon_{hrup}}{\varepsilon_{co}} \right)^{0.45} \quad (9)$$

In Lam and Teng (2003b), k_{s1} and k_{s2} are defined as the shape factors for the strength- and strain-enhancement coefficients which can be calculated by Eqns. 10 and 11, respectively. Here, α and β are given as constant values, 2 and 0.5, respectively by Lam and Teng (2003b). It is worth noting that Eqns. 10 and 11 yield the same result (that is A_e/A_c) for the square sections since $b=h$.

$$k_{s1} = \left(\frac{A_e}{A_c}\right) \left(\frac{b}{h}\right)^\alpha \quad (10)$$

$$k_{s2} = \left(\frac{A_e}{A_c}\right) \left(\frac{h}{b}\right)^\beta \quad (11)$$

$$\frac{\varepsilon_{cc}}{\varepsilon_{co}} = 1.75 + k_2 k_{s2} \left(\frac{f_{lu}}{f_{co}}\right) \left(\frac{\varepsilon_{hrup}}{\varepsilon_{co}}\right)^{0.45} \quad (12)$$

The strength-enhancement ratio (f_{cc}/f_{co}) and strain enhancement ratio ($\varepsilon_{cc}/\varepsilon_{co}$) for all the specimens with square sections are estimated and presented in Table 5.1. Lam and Teng (2003b) states that the rupture strain obtained from the equivalent circular sections should be considered in these predictions. However, the actual rupture strain obtained by testing of the specimens with square sections are also available. Therefore, the strength- and strain-enhancement coefficients are calculated by both considering the rupture strain from the tests of specimens having either the equivalent circular section or square section. The results in Table 5.1 are presented separately for these two cases. The comparison of the experimental results with the corresponding values that were predicted by the Lam and Teng (2003b) model the rupture strain obtained from the tests of specimens having the square sections are given in Figures 5.2 and 5.4. In Figures 5.3 and 5.5, the ultimate conditions are predicted considering the rupture strain obtained from the tests of specimens having equivalent circular sections.

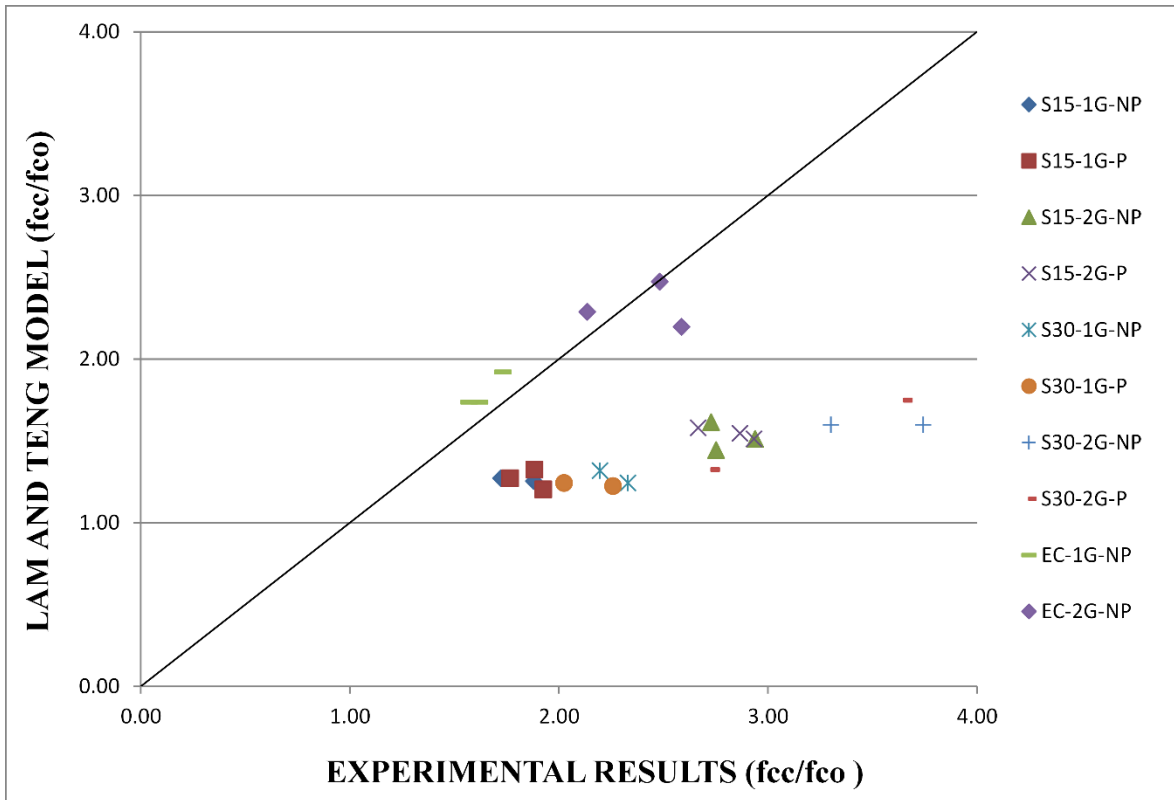


Figure 5.2. Comparison of experimental results and model predictions for strength-enhancement (considering rupture strain from the tests of specimens with square section)

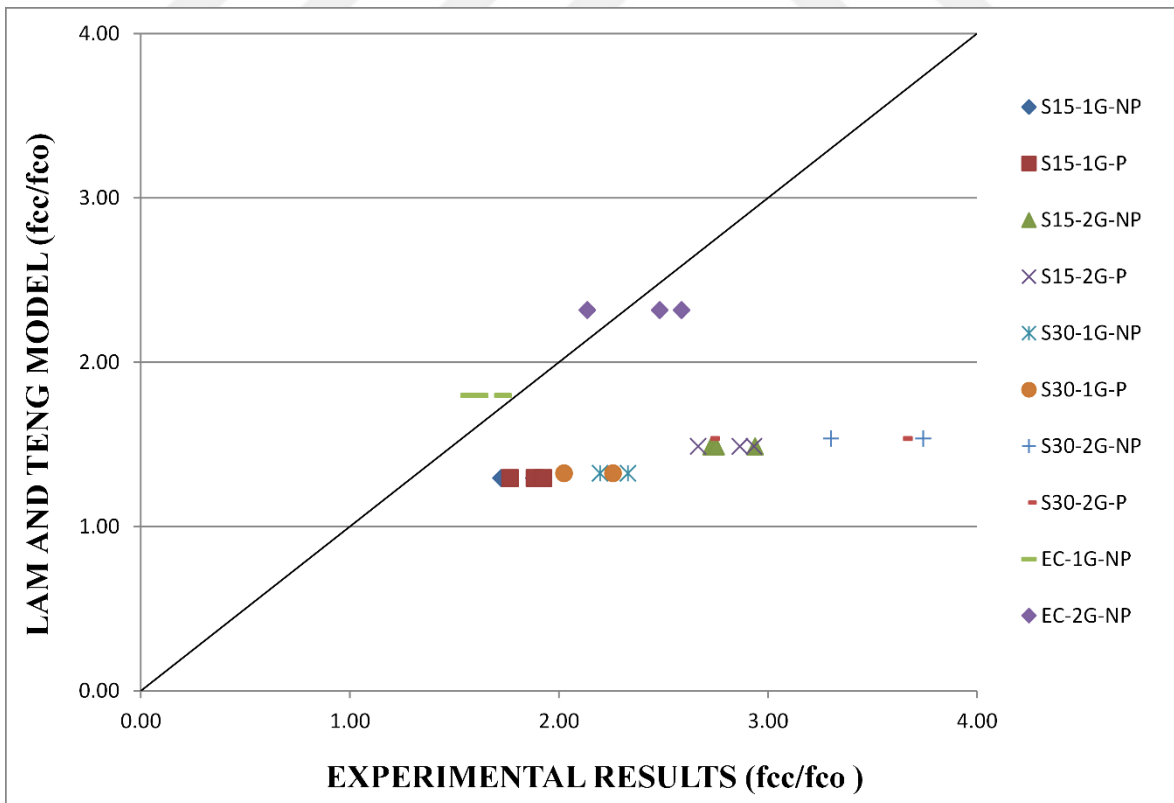


Figure 5.3. Comparison of experimental and model predictions for strength-enhancement (considering rupture strain from the tests of specimens with equivalent circular section)

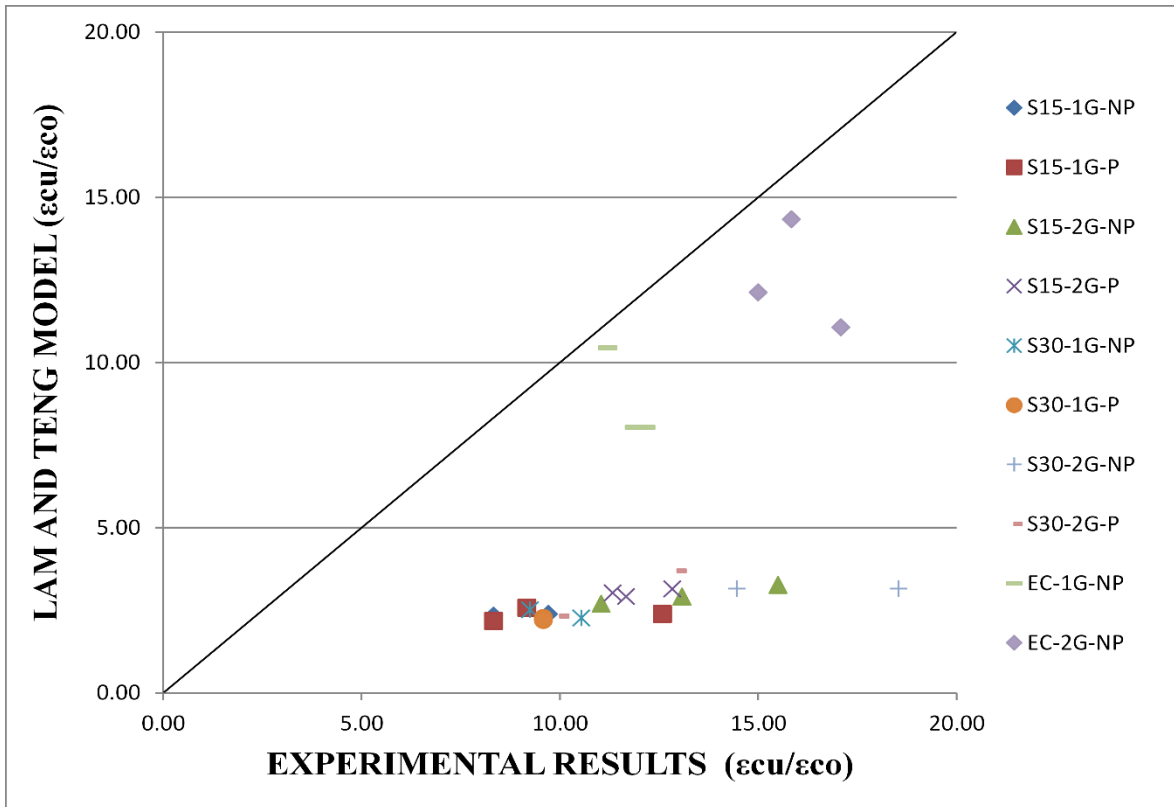


Figure 5.4. Comparison of experimental results and model predictions for strain-enhancement (considering rupture strain from the tests of specimens with square section)

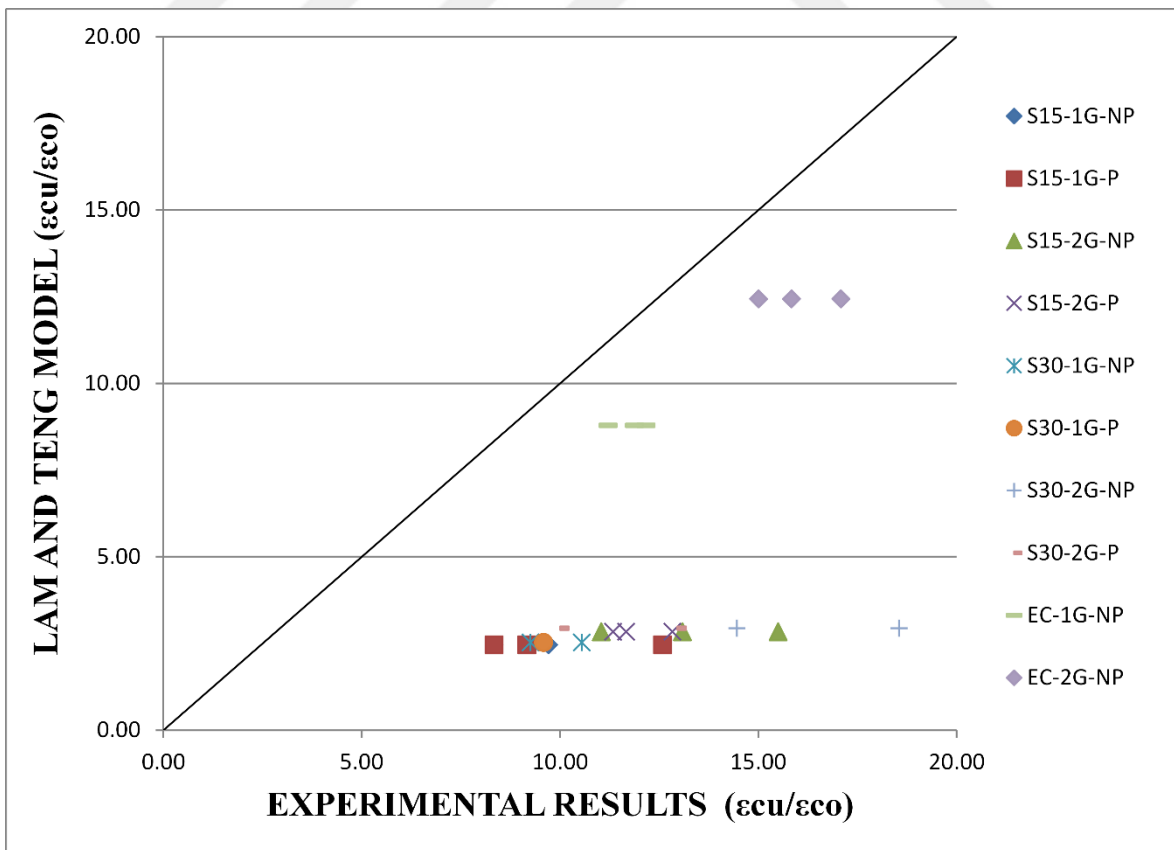


Figure 5.5. Comparison of experimental and model predictions for strain-enhancement (considering rupture strain from the tests of specimens with equivalent circular section)

Table 5.1. The strength- and strain enhancement ratios predicted by Lam and Teng (2003b)

TEST GROUP	SPECIMEN	Experimental Results				Model Predictions					
		Avg. f_{cc}/f_{co}	Avg. $\epsilon_{cu}/\epsilon_{co}$	$\epsilon_{hrup}^{(1)}$	$\epsilon_{hrup}^{(2)}$	$f_{cc}/f_{co}^{(1)}$	Avg. $f_{cc}/f_{co}^{(1)}$	$\epsilon_{cu}/\epsilon_{co}^{(1)}$	Avg. $\epsilon_{cu}/\epsilon_{co}^{(1)}$	$f_{cc}/f_{co}^{(2)}$	$\epsilon_{cu}/\epsilon_{co}^{(2)}$
S15-1G-NP	1	1.80	10.42	0.016	0.0173	1.27	1.27	2.39	2.36	1.30	2.47
	2			NA		NA		NA			
	3			0.015		1.26		2.33			
S15-1G-P	1	1.86	10.03	0.016	0.0173	1.27	1.26	2.39	2.38	1.30	2.47
	2			0.019		1.32		2.57			
	3			0.012		1.20		2.17			
S15-2G-NP	1	2.81	13.21	0.018	0.0143	1.61	1.52	3.27	2.96	1.49	2.84
	2			0.015		1.51		2.92			
	3			0.013		1.44		2.70			
S15-2G-P	1	2.82	11.94	0.015	0.0143	1.51	1.55	2.92	3.03	1.49	2.84
	2			0.016		1.55		3.03			
	3			0.017		1.58		3.15			
S30-1G-NP	1	2.26	9.90	0.013	0.0173	1.24	1.28	2.27	2.40	1.32	2.54
	2			0.017		1.32		2.52			
S30-1G-P	1	2.14	9.58	0.013	0.0173	1.24	1.25	2.27	2.24	1.32	2.54
	2			0.012		1.22		2.21			
S30-2G-NP	1	3.52	16.50	0.016	0.0143	1.60	1.60	3.16	3.16	1.54	2.94
	2			0.016		1.60		3.16			
S30-2G-P	1	3.19	11.48	0.009	0.0143	1.33	1.54	2.33	3.01	1.54	2.94
	2			0.020		1.75		3.69			

(1) The model predictions where the rupture strain of the specimens with square section is considered

(2) The model predictions where the rupture strain of the specimens with equivalent circular section is considered

6. DISCUSSION

6.1. Effect of Corner Radius

It is known that sharp edges negatively affect the axial response in the confinement applications. Figure 4.15, 4.16, 4.17 and 4.18 are presented to show the corner radius effect in different test groups. The results indicate that the strength increases as the corner radius increases. The lowest strength-enhancement ratio was observed in the SRef-2G-NP with sharp edges, although two-layers of GFRP was used for the confinement. In the case of one-layer of GFRP confinement, the axial strength was enhanced by 29 and 15 percent when the corner radius is increased from 15 to 30 mm in the test groups without and with polyurea, respectively. In the two-layers of GFRP confinement, the companion enhancement become to be 25 and 13 percent in the test groups without and with polyurea, respectively. The increase in strength due to the use of larger corner radius in different test groups is also obvious in Figure 4.15, 4.16, 4.17 and 4.18. It may be stated that the strength enhancement is more sensitive to the rounding of the corners with a larger radius in the test groups without polyurea. Besides, strength enhancement due to increasing corner radius seems to be slightly higher for the one-layer of GFRP confinement. The similar results cannot be derived for the axial strain-enhancement due to the higher corner radius. In most of the test groups, the average strain-enhancement ratio of the specimens with 30 mm corner radius are almost equal to those companion specimens with 15 mm corner radius. Furthermore, the strain-enhancement ratio of the SRef-2G-NP was not so different than those of the companion specimens with two-layers of GFRP confinement over a rounded corner.

Although the rupture took place at the corner of SRef-2G-NP as may be expected, the failure was shifted slightly away from the rounded corner in the case of other confined specimens. When the failure types of the specimens with different corner radius are compared, it may be stated that the rupture of the confining jacket becomes more explosive and the ruptured length of the GFRP increased as the corner radius increased.

6.2. Effect of Number of Layers

Figure 4.18 and 4.19 show the effect of the confinement thickness on the axial stress-strain behavior of the specimens with square sections. It is a well-known fact that the confinement efficiency is directly proportional to the number of confining layers. In addition, this effect can be observed more clearly for the low-strength concrete. In the specimens with 15 mm corner radius, the strength-enhancement due to increased confinement thickness (i.e. two layers instead of one layer) was 61 and 52 percent higher for the cases without and with polyurea, respectively. The similar increments become to be 56 and 49 percent in the specimens with 30-mm corner radius for the cases without and with polyurea, respectively. Again, in the test groups where polyurea was applied, the increase in the confinement thickness seem to be slightly less effective in terms of axial strength-enhancement compared to the companion specimens without polyurea. Similarly, the strength enhancement due to increased GFRP thickness was slightly lower in the specimens with 30 mm corner radius compared to those with 15 mm corner radius. The use of larger confinement thickness increased the axial strain capacity in different ratios varying between 1.19 to 1.67. There is no explicit trend to correlate this enhancement with other test parameters.

The type of failure was similar in the one- and two-layers of GFRP confinement when the specimens with 15 mm corner radius are considered. Yet, in the case of test groups with 30 mm corner radius, the rupture was more destructive in the specimens with two-layers of GFRP jacket compared to those with one-layer.

6.3. Effect of Polyurea Coating

The main variable of this study was the use of polyurea under the confining jacket. The expected contribution of polyurea was to serve as a padding material between the core concrete and confining jacket. In this way, it was supposed to protect the FRP sheet from the stress concentrations that may be caused by the deforming concrete and provide a more uniform confinement pressure. Akin et al. (2020) concluded that such an effect could be provided only in the axial cyclic behavior of cylinder specimens with low-strength concrete.

But no such improvement in the axial response could be observed in the monotonic loading. The alleviation of the possible stress concentrations at the corners of the square (or rectangular) specimens in addition to those caused by the deforming concrete under axial loading was mainly aimed in this study.

Figure 4.18 and 4.19 show the effect of polyurea on the overall axial response in different test groups. The results presented in Table 4.1 and Figure 4.18-4.19 clearly reveal that polyurea may have a slight effect when the confinement pressure was low. In the S15-1G test groups, the existence of polyurea (i.e. S15-1G-P compared to S15-1G-NP) provided approximately 6 percent higher axial strength. This effect disappeared as the confinement thickness increased to two-layers or as the corner radius increased to 30 mm. In none of the test groups, the polyurea could result in a higher axial strain-enhancement.

Since the servo-controlled compressive test equipment that is required for cyclic loading was not available in the laboratory, only the monotonic loading could be applied in this study. Besides, only GFRP confinement could be applied since the axial load capacity of the available system was not adequate for the higher strength enhancement that may be provided by the use of other FRP's. The results under monotonic axial loading for the GFRP confined low-strength concrete with square sections repeated the results of Akin et al. (2020) under same type of loading which had been for the cylindrical low-strength CFRP confined concrete specimens. Yet, as it was concluded in that previous study, the results may change under cyclic axial loading. On the other hand, the use of other types of FRP materials may lead to different results in this regard.

6.4. Comparison with the Existing Model

The stress- and strain-enhancement ratio (f_{cc}/f_{co} and $\epsilon_{cc}/\epsilon_{co}$) was calculated in two ways according to Lam and Teng (2003b). Table 5.1 shows the stress- and strain-enhancement ratios calculated with the hoop rupture strain (ϵ_{hrup}) measured during the tests of either the actual specimens with square sections or those with equivalent circular sections. The experimentally obtained axial strength- and strain-enhancement ratios were also provided in this table. Figures 5.2, 5.3, 5.4 and 5.5 include the comparison of the experimental results with the model predictions.

The comparison of the results indicate that Lam and Teng (2003b) model predicted the ultimate strength considerably lower compared to the test results in all cases. The difference in the predicted and experimental results seems to increase as the confinement thickness and related confining pressure increases. Again the difference of the experimental and model predicted axial strength was larger in the specimens with 30 mm corner radius compared to the those with 15 mm corner radius. There seems to have no effect of polyurea in the accuracy of the model predictions.

Similar to axial strength, the ultimate strain capacity predictions of Lam and Teng (2003b) were smaller compared to the experimentally achieved values in all cases. However, the underestimation of the axial strain capacity by the model predictions was much more significant compared to those of the axial strength. The test parameters seem to have no influence on this underestimation.

Lam and Teng (2003b) model for the square/rectangular sections was based on the Lam and Teng (2003a) model that had been for the circular sections. And Lam and Teng (2003a) model has proven its accuracy for different cases with varying parameters. The inaccuracy of Lam and Teng (2003b) model for the specimens of this study with square sections may be attributed to the shape factors for the strength- and strain-enhancement coefficients (k_{s1} and k_{s2} , respectively). There may be a need for the modification of the definition of these parameters especially for the confinement of low-strength concrete.

7. CONCLUSIONS

In this thesis, the axial compressive behavior of low strength concrete that was confined with GFRP has been presented. The constitution of a polyurea layer on the square concrete surface before wrapping by the GFRP sheet was the main concern of the study. The polyurea layer was supposed to serve as a padding layer between the concrete and confining jacket. Thus, the unfavorable effect of stress concentrations produced not only due to deforming concrete under axial loading but also those formed at the corners of the square section were aimed to be reduced. An experimental study was conducted in this regard by testing 29 concrete specimens in total. The other test parameters which were considered in the experimental study were the corner radius which was applied for rounding the sharp edges of square sections and number of GFRP layers. Besides, the test results in terms of ultimate strength and strain were compared with the predictions of the design-oriented Lam and Teng (2003b) model.

The following conclusions were summarized according to the results. These conclusions should not be generalized without due judgement or unless they were supported by further experimental findings.

1. In the confinement of low strength concrete by GFRP, the rounding of the corners of the columns positively affects the axial compressive strength of the concrete. As the corner radius applied for rounding was increased, the increment of strength provided by the GFRP confinement was also advanced. This advancement was slightly better in the case of lower confining pressure of the one-layer of confinement compared to that of two-layers. Besides, the enhancement of strength provided by rounding the corners with a larger radius was higher in the test groups without polyurea.

2. The rounding of the edges by 15 or 30 mm corner radius did not alter the ultimate axial strain capacity attained by the GFRP confinement, as opposed to the conclusion for the strength-enhancement. This inference was valid in all test groups with varying parameters (i.e. existence of polyurea or confinement thickness).

3. The rounding of the edges shifted the rupture slightly away from the corners which was the case in the specimen SRef-2G-NP. The increased corner radius caused a more explosive type failure with a larger rupture zone.

4. The increased confinement thickness (i.e. two-layers instead of one-layer) enhanced the ultimate axial strength with varying ratios. The highest enhancement was observed in the test groups with 15 mm corner rounding and without polyurea. The strength-enhancement was slightly less effected by the increase of the confinement thickness for the specimens with polyurea.

5. The increased confinement thickness also enhanced the axial strain capacity with varying ratios between 19 and 67 percent. However, this enhancement seems not to be correlated with other test parameters considered in this thesis study.

6. The type of failure was identical in the one- and two-layers of confinement for the test groups with 15 mm corner radius. However, the increased confinement thickness caused a more destructive (i.e. more explosive with a larger rupture zone) failure for the test groups with 30 mm corner radius.

7. The polyurea increased the ultimate axial strength slightly (i.e. by 6 percent) in the test groups with one-layer of confinement having a corner radius of 15 mm. However, this enhancement seems to vanish as the number of GFRP layers or the corner radius increase. The polyurea could not cause an alteration of the ultimate axial strain capacity in any of the test groups. It should be noted that this conclusion was obtained from the monotonic test results of specimens with square sections. A similar conclusion was also reported by Akin et al. (2020) for the specimens with circular sections. However, the same study also stated that the ultimate strain capacity could be enhanced considerably in the case of cyclic loading. The same statement may be valid for the specimens with square sections which requires an experimental validation.

8. The Lam and Teng (2003b) model underestimated the axial strength and strain capacity of all test specimens significantly. The underestimation of the axial strength was even more significant for the larger corner radius and confinement thickness. The polyurea had no effect in this regard. The underestimation was much more severe for the axial strain capacity where no correlation can be defined by considering different test parameters.

9. The model of Lam and Teng (2003b) for the square and rectangular sections was based on the Lam and Teng (2003a) model that had been for the circular sections. Lam and Teng (2003b) model has proven its efficiency to predict the ultimate conditions of the FRP confined concrete with circular sections accurately in many different cases including low-strength concrete. The only differences of Lam and Teng (2003b) model from its precessor

is the strength- and strain-enhancement coefficients (k_{s1} and k_{s2} , respectively). The inaccuracy of the model predictions may be attributed to these coefficients, especially for the low-strength concrete. Therefore, further studies are required to verify this conclusion by a consideration of various parameters. These coefficients may need to be modified after such a study.



8. REFERENCES

- ACI Committee 440 Report (2002). Guide for the design and construction of externally Bonded FRP systems for strengthening concrete structures, American Concrete Institute (ACI) Committee 440, Technical Committee Document 440.2R-02
- Akin, E., Tunaboyu, O., Avsar, O., (2020). Axial behavior of FRP confined low-strength concrete with polyurea. *Structures*, 28:1774-1778. doi:10.1016/j.istruc.2020.10.015
- Al-Salloum, Y., (2007). Influence of edges sharpness on the strength of square concrete column confined with FRP composite laminates, *Elsevier Science Direct-Composites*, part-B38, pp:640–650. doi:10.1016/j.compositesb.2006.06.019
- Altin, M. (2008). Cost analysis in educational buildings strengthened with reinforced concrete shear wall addition and column sheathing method, Doctorate Thesis, Selcuk University Institute of Science, Konya.
- ASTM C39/C39M–20 (2020). Standard test method for compressive strength of cylindrical concrete specimens, ASTM International, West Conshohocken, PA.
- ASTM D3039-17, (2017). Standard test method for tensile properties of polymer matrix composite materials, ASTM International, West Conshohocken, PA.
- Bakis, C.E., Bank, L.C., Brown, V.L., Cosenza, E., Davalos, J.F., Lesko, J.J., ...Triantafillou, T.C., (2002). Fiber-reinforced polymer composites for construction state-of-the-art review, *Journal of Composites for Construction*, ASCE, 6(2):73-87. doi:10.1061/(ASCE)1090-0268(2002)6:2(73)
- Ballinger, C. A., (1997, May 4-8). *42nd International SAMPE Symposium: strengthening of engineering structures with carbon fiber reinforced plastics- an overview of history and current worldwide usage*, pp: 927-932.
- Buyukozturk, O., (2000, July 5). *Symposium on Earthquake Engineering: repair and strengthening of reinforced concrete structures* [conference presentation]. Professional Engineering Society (IMO), Istanbul, Turkey.
- Cao, Q., Lv, X., Wang, Y., Wu, Z., Lin, Z., (2020). Performance and analysis of unidirectional GFRP actively confined high-strength concrete under monotonic and

cyclic axial compression, *Elsevier Construction and Building Materials*, 0950-0618.
doi:10.1016/j.conbuildmat.2020.121593

CEB Task Group 9_3 (2001) Technical report-externally bonded FRP reinforcement for RC structures, Bulletin No 14, International Federation for Structural Concrete (fib), Lausanne.

Chaallal, O., Hassan, M., Shahawy, M. (2003). Confinement model for axially loaded short rectangular columns strengthened with fiber-reinforced polymer wrapping, *ACI Structural Journal*, 100(2): 215-221. doi:10.14359/12485

Fardis, M.N. and Khalili, H. (1982). FRP encased concrete as a structural material, *Magazine of Concrete Research*, 34(112). doi:10.1680/mac.1982.34.121.191

Fukuyuma, H., Nakai, H., Tanigaki, M., Uomoto, T., (1997). *Proceedings of the Third International Symposium: non-metallic (FRP) reinforcement for concrete structures*, JCI State of the Art on Retrofitting by CFRM Part 1. Materials, Construction and Application, Japan, pp: 605-612.

Kobatake, Y., (1998). A seismic retrofitting method for existing concrete structures using CFRP, *Advanced Composites Materials*, Vol.7, No. 1, pp:1-22.
doi:10.1163/156855198X00011

Koksal, H. O., and Doran, B., (2009). Stress-strain model of Square/Rectangular concrete columns confined with FRP sheets, *Submitted to Engineering Structures Manuscript*.

Lam, L., Teng, J.G. (2003a.). Design-oriented stress-strain model for FRP-confined concrete. *Construction and Building Materials*, 17, 471-489.
doi:10.1016/S09500618(03)00045-X

Lam, L., Teng, J.G., (2003b). Design-oriented Stress-Strain Model for FRP-confined concrete in rectangular columns. *Reinforced Plastics and Composites*, 22, 1149–38.
doi:10.1177/073168403035429

Mirmiran, A., Shahawy, M., Samaan, M., EI Echary, H., Mastrapa, J.C., Pico, O., (1998). Effect of column parameters on FRP-confined concrete. *Composite for Construction*, 2, pp:175-185. doi:10.1061/(ASCE)1090-0268(1998)2:4(175)

Miyauchi, K., Inoue, S., Korda T., Kobayashi A., (1999). Strengthening effect of draft concrete columns with carbon fiber sheet, *Transactions of the Japan Concrete Institute*.

- Ozbakkaloglu, T., Akin, E., (2012). Behavior of FRP-confined normal- and high-strength concrete under cyclic axial compression. *Journal of Composites for Structures*, vol. 16, no. 4, pp: 451–463. doi:10.1061/(ASCE) CC.1943-5614.0000273
- Ozbakkaloglu, T., Oehlers, D. J., (2008). Concrete-filled square and rectangular FRP tubes under axial compression, *Journal of Composites for Structures*, 12(4), pp: 469-477. doi:10.1061/(ASCE)1090-0268(2008)12:4(469).
- Ozcan, O., Bıncı, B., Özcebe G., (2010). Seismic strengthening of rectangular reinforced concrete columns using fiber reinforced polymers. *Elsevier Engineering Structures*, vol. 32, no. 4, pp: 964- 973. doi:10.1016/j.engstruct.2009.12.021
- Paula, R. F., Silva, M. G., (June 2002). *Third International Conference on Composites in Infrastructure Conference: sharp edge effects on FRP confinement of RC square columns.*
- Priestley, M. J. N., Seible, F., Calvi, G. M., (1996). Seismic design and retrofit of bridges, *John Wiley & Sons Inc*, New York.
- Saadatmanesh, H., Ehsani, M.R. and Li, M. W., (1994). Strength and ductility of concrete columns externally reinforced with fiber composite straps, *ACI Structural Journal*. doi:10.14359/4151
- Santos, L. S. de, Damasceno, I. I. R., Ribeiro, L. C. N., Oliveira, D. R. C. de., (2013). Rounded corners columns strengthened with CFRP. *Acta Scientiarum. Technology*, 35(3), pp: 463-468. doi:10.4025/actascitechnol.v35i3.15124
- Sharma, S. S., Daveb, U. V., Solankic, H., (2013). FRP wrapping for RC columns with varying corner radii, *Elsevier Procedia Engineering*, no: 51, pp: 220-229. doi:10.1016/j.proeng.2013.01.031
- Stylianidis, P. M., Petrou, M. F., (2019). Study of the flexural behavior of FRP-strengthened steel-concrete composite beams, *Elsevier Structures*, no: 22, pp: 124-138. doi:10.1016/j.istruc.2019.07.012
- Tankut, T., (2005, September). *Congress on Civil Engineering Problems of Antalya Region: strengthening strategy for building in Turkey*, congress symposium proceedings book.
- Tao, Z., Yu, Q., Zhong, Y. Z., (2008). Compressive behavior of CFRP-confined rectangular concrete columns, *Magazine of Concrete Research*, 60, No: 10, pp: 735–745. doi:10.1680/mac.2007.00115

- Toy, T.A., (2008). Behavior of square and rectangular sections concrete columns confined with polymers. Master Thesis, Yildiz Technique University, Institute of Science, Department of Civil Engineering, 96s, Istanbul.
- Turkish Earthquake Codes (2018). Republic of Turkey Prime Ministry Disaster and Emergency Management Authority, Official Gazette, No: 30364, 18 March 2018.
- Wang, L. M., Wu, Y. F., (2008). Effect of corner radius on the performance of CFRP confined square concrete columns, *Engineering Structures*, no: 30, pp: 493–505. doi:10.1016/j.engstruct.2007.04.016
- Wu, G., Lu, Z. T., Wu, Z. S., (2006). Strength and ductility of concrete cylinders confined with FRP composites, *Construction and Building Materials*, 20, pp: 134-148. doi:10.1016/j.conbuildmat.2005.01.022
- Yang, X., Nanni A., and Chen, G., (2001). Effect of corner radius on performance of externally bonded FRP reinforcement, non-metallic reinforcement for concrete structures - FRPRCS-5, Cambridge, July 16-18, 2001, pp. 197-204.
- Yilmaz, B., (2006). Repair and strengthening of reinforced concrete structures: controlled demolition by using explosives in case of uneconomical reinforcement. Master Thesis, Osmangazi University, Institute of Science, Department of Civil Engineering, 121s, Eskisehir.
- Zhong, Y. Z., Yu, Q., Tao, Z., (2008). Compressive behavior of CFRP-confined rectangular concrete columns, *Magazine of Concrete Research*, vol. 60, no: 10, 735–745. doi:10.1680/macr.2007.00115

REPUBLIC OF TURKEY
AYDIN ADNAN MENDERES UNIVERSITY
GRADUATE SCHOOL OF NATURAL
AND APPLIED SCIENCES
AYDIN

I hereby declare that I composed all the information in my master's thesis entitled AXIAL BEHAVIOR OF FRP CONFINED SQUARE COLUMNS WITH POLYUREA within the framework of ethical behavior and academic rules, and that due references were provided and for all kinds of statements and information that do not belong to me in this study in accordance with the guide for writing the thesis. I declare that I accept all kinds of legal consequences when the opposite of what I have stated is revealed.

.../.../20..

Selin TAYLAN